Defense Special Weapons Agency
Alexandria, VA 22310-3398

DNA-TR-95-68

Space Power Experiments Aboard Rockets
SPEAR-3

W. John Raitt
Utah State University
Center for Atmospheric & Space Sciences
Logan, UT 84322-4405

July 1997

Technical Report

19970717 180

DTIC QUALITY INSPECTED 3

DESTRUCTION NOTICE:

DSWA

DISTRIBUTION LIST UPDATE

This mailer is provided to enable DSWA to maintain current distribution lists for reports. (We would appreciate your providing the requested information.)

☐ Add the individual listed to your distribution list.

☐ Delete the cited organization/individual.

☐ Change of address.

NAME: _____

ORGANIZATION: _____

OLD ADDRESS	**CURRENT ADDRESS**
_____	_____
_____	_____
_____	_____

TELEPHONE NUMBER: ( ) _____

DSWA PUBLICATION NUMBER/TITLE	**CHANGES/DELETIONS/ADDITIONS, etc.)** *(Attach Sheet if more Space is Required)*
_____	_____
_____	_____
_____	_____

DSWA OR OTHER GOVERNMENT CONTRACT NUMBER: _____

CERTIFICATION OF NEED-TO-KNOW BY GOVERNMENT SPONSOR (if other than DSWA):

SPONSORING ORGANIZATION: _____

CONTRACTING OFFICER OR REPRESENTATIVE: _____

SIGNATURE: _____

CUT HERE AND RETURN

DEFENSE SPECIAL WEAPONS AGENCY
ATTN: IMAS
6801 TELEGRAPH ROAD
ALEXANDRIA, VA   22310-3398

REPORT DOCUMENTATION PAGE

Form Approved
OMB No. 0704-0188

1. AGENCY USE ONLY (Leave blank)	2. REPORT DATE 970701	3. REPORT TYPE AND DATES COVERED Technical 910411 - 941115

4. TITLE AND SUBTITLE
Space Power Requirements Aboard Rockets
SPEAR-3

6. AUTHOR(S)
W. John Raitt

5. FUNDING NUMBERS
C   - DNA 001-90-C-0166
PE - 62715H
PR - SF
TA - SD
WU - DH307820

7. PERFORMING ORGANIZATION NAME(S) AND ADDRESS(ES)
Utah State University
Center for Atmospheric & Space Sciences
Logan, UT 84322-4405

8. PERFORMING ORGANIZATION REPORT NUMBER

9. SPONSORING/MONITORING AGENCY NAME(S) AND ADDRESS(ES)
Defense Special Weapons Agency
6801 Telegraph Road
Alexandria, VA 22310-3398
RAST/Filios

10. SPONSORING/MONITORING AGENCY REPORT NUMBER

DNA-TR-95-68

11. SUPPLEMENTARY NOTES
This work was sponsored by the Defense Special Weapons Agency under RDT&E RMC Code B7664D SF SD 00312 1950A 25904D. Additional support and funding provided by the Ballistic Missile Defense Organization.

12a. DISTRIBUTION/AVAILABILITY STATEMENT

Approved for public release; distribution is unlimited.

12b. DISTRIBUTION CODE

13. ABSTRACT (*Maximum 200 words*)

The SPEAR-3 program was a sounding rocket payload designed to study the interaction of a charged body with the Earth's upper atmosphere with particular reference to the discharging ability of selected active devices carried on the payload. Since some of the devices and natural outgassing provide a source of gaseous effluent release, instrumentation was included to study effluent dispersion around the payload. It was found that neutral gas release was most effective at discharging the payload when it was more negative than ~500 V. Electron emission was effective only when the currents driving the body negative were lower than the limited current available from the low perveance devices used. The hollow cathode was an ineffective grounding system on this flight due to cathode poisoning believed to have occurred during the vehicle ascent. The grounding data and HV interactions were diagnosed by a variety of instruments measuring both steady state and transient currents and voltages.

14. SUBJECT TERMS
SPEAR-3
Space Power
Rocket Payload
Vehicle Charging
Diagnostic Testing
High Voltage Interaction

15. NUMBER OF PAGES
70

16. PRICE CODE

17. SECURITY CLASSIFICATION OF REPORT UNCLASSIFIED	18. SECURITY CLASSIFICATION OF THIS PAGE UNCLASSIFIED	19. SECURITY CLASSIFICATION OF ABSTRACT UNCLASSIFIED	20. LIMITATION OF ABSTRACT SAR

NSN 7540-280-5500

Standard Form 298 (rev. 2-89)
Prescribed by ANSI Sta. 239-18
298-102

CLASSIFIED BY:

N/A since Unclassified.

DECLASSIFY ON:

N/A since Unclassified.

SUMMARY

The SPEAR-3 science-oriented sounding rocket payload was initiated as a follow-on to the previous two payloads in the SPEAR program. It was designed to answer questions raised by the SPEAR-1 project with respect to HV space-environment interactions in general and the effectiveness of active systems in reducing the vehicle charge and hence its potential with respect to its environment. Associated with the relief of electrical charging, the dispersion of released effluents in some of the active sub-systems was another objective of the mission. The focus of the experiments on SPEAR-3 was on different methods of discharging, or grounding, the payload to study means of controlling the potential of low-earth-orbit satellites which have been observed to charge to high negative potentials when traversing the Earth's auroral zones.

The SPEAR-1 biasing arrangement of applying a potential between a deployed sphere and the payload structure was used to design a payload which would reach maximum potentials up to 2 kV negative relative to its surroundings, thereby simulating the maximum potentials observed in low-earth-orbit vehicles resulting from natural charging mechanisms. Two general categories of grounding devices were included in the payload: Electron emission systems to physically eject the surplus electrical charge; and effluent emitting systems to enhance the plasma density in the vicinity of the charged body.

One of the electron emitting devices was a conventional thermionic emitter, but using a tungsten filament rather than an activated cathode to avoid the poisoning effect of contaminants at the payload surface. The other device used a developing technology of field emission from arrays of very sharp points induced to emit electrons by very high electric fields at the small radius tips.

The effluent emission devices were a hollow cathode plasma contactor designed to emit plasma by internal ionization of a flowing stream of argon gas and a neutral gas release system which could emit nitrogen gas from four nozzles arranged to produce no disturbing torques or forces on the payload.

In addition to the means of charging the vehicle and the systems to attempt to discharge it to the Earth's ionosphere, the payload carried an array of diagnostic devices to help interpret the physical mechanisms involved in the discharging effect. Two vehicle potential measuring devices were included, one using a floating probe which was located on a boom to be outside the vehicle charge sheath at voltages below about 300 V, and another to measure the spectra of ions accelerated into the vehicle by negative potentials from ~50 V up to ~5000 V induced by the charging system. Additional experiments were included to study the dispersion of released effluents by optical imagery of light from excited states of the effluent, to study the effect of the high negative potentials on different types of solar cells and to monitor both steady and transient currents and voltages. The ambient environment was monitored by a Langmuir probe for electron density, and a cold cathode ionization gauge to measure the neutral pressure close to the payload skin.

The conclusions obtained for the experiments on grounding the payload were that the gas emission was always effective at discharging the payload for potentials more negative than ~500 V. The electron emission devices worked when the ionospheric plasma density was low enough that their emitted currents exceeded the electrons being collected by the deployed sphere being used to drive the payload negative. The hollow cathode plasma contactor was ineffective at discharging the payload because of a suspected failure of the cathode resulting from poisoning of its surface when the ground gas purge system was removed just before launch. The effect of early dispersion of effluents was deduced from external breakdown in the gas cloud surrounding the payload on the upleg which was not apparent on the downleg. No imagery of this effect or the ionization associated with the gas release system was obtained due to the failure of one of the telemetry transmitters carrying two camera signals.

In summary, the SPEAR-3 mission was successful considering the complexity of the payload which represented the limit obtainable in a Black Brant sized payload. The most significant failures were the loss of the LLLTV telemetry transmitter and the failure of the hollow cathode system to generate plasma. Despite these setbacks, the payload demonstrated the capabilities of grounding negatively charged space platforms, and contributed to our knowledge in general of the interaction of charged bodies with the upper atmosphere.

CONVERSION TABLE

Conversion factors for U.S. Customary to metric (SI) units of measurement

MULTIPLY ⟶	BY ⟶		TO GET
TO GET ⟵	BY ⟵		DIVIDE
angstrom	1.000 000	XE -10	meters (m)
degree (angle)	1.745 329	XE -2	radian (rad)
degree Fahrenheit	$T_K = (T\ °F + 459.67)/1.8$		degree kelvin (K)
electron volt	1.602 19	XE -19	joule (J)
inch	2.540 000	XE -2	meter (m)
mile (international)	1.609 344	XE +3	meter (m)
ounce	2.834 952	XE -2	kilogram (kg)
pound-force/inch²(psi)	6.894 757		kilo pascal (kPa)
torr (mm Hg, 0° C)	1.333 22	X E -1	kilo pascal (kPa)

TABLE OF CONTENTS

FIGURES

SECTION 1

INTRODUCTION

The Space Power Experiments Aboard Rockets (SPEAR) program was initiated in 1985 by the Strategic Defense Initiative Office, Innovative Science and Technology division (SDIO/IST) and has been managed by the Defense Nuclear Agency (DNA) to study the interaction of electrically charged space platforms and space flight components with the low-earth-orbit (LEO) environment. The principal objective of the SPEAR-3, the third mission in the series, was to study the interaction of a differentially charged space platform with the upper atmospheric environment with and without active devices to reduce the impedance of the negative element to the ionosphere. An additional objective was to study the dispersion of effluents used in that category of impedance reducing systems (*Raitt et al.,* 1995a).

A Black Brant 9A sounding rocket successfully launched SPEAR-3 on March 15, 1993, from NASA's Wallops Flight Facility, VA. The payload was launched at 21:12:41 EST, the payload reached an apogee of 289 km. All mechanical systems functioned as planned, and the attitude maneuvering system completed its program of orienting the payload in different directions relative to the geomagnetic field.

The interaction between electrically biased parts of the payload results from the presence of the ionosphere at LEO altitudes. This region is a weakly ionized plasma, and as such it will allow currents to flow from/to those parts of the system biased relative to the plasma. The current flow from the positive parts is determined by electron collection, while that to the negative parts is determined by ion collection and secondary electron emission. The collecting characteristics for the two polarities are quite different because of the large mass difference between the ions and the electrons and the high yield of secondary electrons from energetic ion impact on metal surfaces.

To explore the HV interaction, SPEAR-3 was similar in configuration to SPEAR-1 in that the electrical biasing potentials of the system were determined by connecting a charged capacitor between a boom-deployed sphere and the rocket body with polarity such that the sphere was driven positive and the body negative relative to the ambient ionosphere. The principal objective of the flight was to use the negative bias on the body to simulate the highest degree of electrical charging seen on polar orbiting satellites at ~800 km altitude, and then test different means of reducing the potential of the vehicle, that is, grounding it to the ionosphere. The grounding devices were categorized into two basic types, one emitting electrons to reduce the charge on a negative object, the other emitting neutral or ionized effluent from the charged body and relying on local ionization of the enhanced effluent density around the vehicle to provide increased plasma currents to discharge the vehicle. The use of effluent release allowed experiments to be performed to study the effectiveness of the enhanced effluent density around the vehicle to diminish localized differential charging of surfaces.

This report describes the SPEAR-3 science objectives, the payload instrumentation and mission plan designed to achieve the science objectives, the results of the flight performance, and the implications regarding the effectiveness of the grounding devices.

1

SECTION 2
SCIENCE OBJECTIVES

The overall science objectives of the mission were as follows:

1. To test a variety of space platform grounding schemes for bias levels up to ~2 kV negative potential as a function of:

   (i) Altitude in LEO region

   (ii) Attitude relative to geomagnetic field

   (iii) Different bias levels

2. To diagnose the physics of the operation of the grounding devices

3. To study the dispersion of gaseous effluent emitted from a space platform

4. To study the effects of high bias voltages on the performance of a solar cell module in the presence of emitted gaseous effluents

5. To test the effectiveness of the grounding techniques in reducing local differential charging on a diagnostic probe and on solar cells

6. To monitor the undisturbed and disturbed plasma and neutral gas environments of the payload

SECTION 3

INSTRUMENTATION DESCRIPTION

3.1 HIGH VOLTAGE SYSTEM.

The high voltage to bias the vehicle, and to provide sufficient current to ground it to the ionosphere was derived from a capacitor charged to 10 kV from a high voltage power supply. Since the current capacity of the power supply resulted in a charging time of ~4 secs for the 2 µF capacitor used, two capacitors were employed so that while one was being used to charge the vehicle, the other was being charged from the power supply. The time periods of the charge and discharge periods were such that a fully charged capacitor was available as soon as a discharge cycle was completed. In addition to the switching to accomplish the charge and discharge phases, additional switching was included to either apply the voltage "instantaneously", i.e., over the time period represented by relay closure, or to ramp up the voltage over a time period of 10s of mS by an RC network. The two methods of applying the differential bias were alternated throughout the flight.

The high voltage system included monitors of the biasing voltage as well as the currents flowing through the branches of the system, from which the current flowing from the ionosphere to the vehicle could be deduced.

3.2 GROUNDING DEVICES.

The four grounding devices referred to earlier were tested on the payload in synchronism with the application of the vehicle bias voltage. The independently operating Attitude Control System (ACS) provided additional short periods of effluent release when the control jets operated, releasing nitrogen.

3.2.1 Neutral Gas Release System.

The Neutral Gas Release System (NGRS) consisted of two pairs of horizontally opposed jets with axes of symmetry tangent to a cross section of the payload skin. The gas flows in the four jets were closely matched, so that no significant torques or thrusts resulted from the programmed gas releases.   A regulator reduced the tank pressure to a line pressure with gas flowing of ~200 psi, and a single valve for each pair of nozzles mounted close to the nozzles controlled the gas releases. This reduced the residual outgassing of the system once the gas was cut off. An additional regulator gave a lower flow rate for half of the gas releases. The flow rates were 2 g/sec per nozzle at the high level and 0.2 g/sec at the low level. Most gas pulses were 100 msec, but each discharge sequence was initiated with a 200 msec pulse. The gas used was argon. Figure 3-1 illustrates the mechanical design of the region near one pair of jets as well as an enlarged view of one of the screw-in nozzles. Each nozzle had a throat diameter of .74 mm and an exit diameter of 1.75 mm to give an exit velocity of Mach 4.

3.2.2 Hollow Cathode Plasma Contactor (HCPC).

The plasma contactor grounding device (HCPC) was designed to produce a plume of plasma at its orifice by ionizing xenon gas flowing through the electron flux produced in the hollow cathode. The orifice was deployed to be outside the plane of the vehicle skin, and the axis of symmetry was in a radial direction. Provision was made to pre-heat the cathode on the ascent part of the trajectory, thereby allowing a fast start-up once operating altitude was reached. In addition to the plasma generated, the hollow cathode emitted neutral xenon, but at a much lower flow rate than the gas release system. The current capacity of the hollow cathode was designed to be at least 10 amperes for either ion or electron collection. Figure 3-2 is a drawing of the cathode assembly.

3.2.3 Thermionic Emitter (TE).

A heated tungsten filament with a saturation emission current capacity of 1.2 amperes (TE) was mounted to be exposed just below the plane of the vehicle skin after door deployment. The normal to the disc shaped cathode was oriented to be in a radial direction. The cathode was constructed using a Tungsten/Rhenium alloy (97/3 %) wire. The cathode was heated by an alternating current at a frequency of 2.0 kHz. The electrons were accelerated into the charge sheath around the vehicle by a 15 volt negative bias applied to the cathode. Although the cathode was just below the plane of the skin, it was located in a

3

well that was nine times the diameter of the filament disc. Figure 3-3 shows the mechanical assembly of the thermionic emitter filament, which is in the shape of a "potato masher."

3.2.4 Field Emission Device.

The Field Emission Device (FED) was designed to emit electrons on the application of an electric field to very-small-radius points fabricated on a substrate. Each individual device was housed in a TO-5 transistor can, and the driving electronics were designed to set the maximum emitted current at 10 mA per device. A total of nine devices were used to provide a maximum capacity of 90 mA from the unit. Control of the device was achieved by the application or removal of the voltage to an integrated electrode over the points used to produce the extraction electric field necessary for field emission ($80V < V < 200V$). Figure 3-4 gives (a) a schematic and (b and c) micrographs of a prototype FED device.

3.3   DIFFERENTIAL SURFACE CHARGING.

One of the objectives was to study the influence of the effluent releases on the reduction of differential charging on surfaces mounted on the vehicle. This was achieved by two devices. In one the differential charge was deliberately applied, and in the other the observed tendency for solar cells to develop regions of localized charge build-up when negatively biased relative to a plasma was exploited.

3.3.1   Differential Charge Device (DCD).

This device (DCD) consisted of an isolated metal plate capable of being charged 2000 volts more negative than the skin of the vehicle. The size of the plate was 90 x170 mm, and it was made of the same material as the vehicle skin and underwent the same surface finishing process (alochrom). The potential of the plate was monitored as it was allowed to discharge back to vehicle skin potential through the external plasma environment. The impedance of the voltage monitor and a fixed shunt capacitor set the decay time constant of the device to be ~500 msec in the absence of external plasma. Figure 3-5 is a block diagram of the DCD electrical system, and Figure 3-6 shows the mechanical layout of the DCD.

3.3.2   Solar Cell System.

An assembly of four different types of solar cell arrays were mounted to a metal baseplate which was deployed into the vehicle sheath at operating altitude. Two of the cell arrays were the type planned for the Space Station, the other two were advanced design gallium arsenide cells. Provision was made to count pulses of current associated with discharges from the individual cell arrays and also to test the operation of the cells by periodically illuminating them with a light source. The steady current generated by the illumination and the plasma current to the biased cells was also measured. The biasing range for the solar cells was extended by adding a positive bias source at 500 volts, which overcame the vehicle bias part way through its sweep and resulted in the solar cells being positively biased relative to the plasma. The location of the arcs on the solar cells was planned to be observed by a Low Light Level Television (LLLTV) directed at the deployed array and sensitized only when the cell illumination was off. Figure 3-7 shows the deployed position of the solar cell system as viewed from above. Each of the shapes on the rectangular area represents a solar cell.

3.4   VEHICLE POTENTIAL.

3.4.1   Electrostatic Analyzer.

The Electrostatic Analyzer (ESA) measured the energy of positive ions arriving at its aperture in the energy range 10 eV to 25 keV using a pair of sensors to split the total energy range into 10 - 750 eV and 0.33 - 25 keV. The shape of the spectrum of ion energy should peak at the energy given to those ions accelerated through the vehicle sheath and therefore provide a measure of the electrostatic potential of the vehicle relative to the undisturbed plasma. The energy resolution of the instrument was 7%, and the sweep time was 32 msec using 64 energy steps of 500 μsec duration. Two sensor pairs with different entrance aperture sizes provided a total dynamic range of ion flux from 0.2 - 2000 $\mu A/m^2$. The field of view of each sensor was 20° x 5° about a radial direction, with the direction of the wider field of view parallel to the longitudinal axis of the vehicle. Figure 3-8 is a block diagram of the ESA, and Figure 3-9 is drawing of an assembled sensor.

3.4.2 Floating Probe

The floating probe system was designed to provide vehicle potential measurements at the lower end of the expected range with higher time resolution than the ESA. The probe was a 64 mm diameter aluminum sphere mounted on a 2.5 m Weitzmann boom extended when the payload reached operational altitude. The surface of the boom had a conducting bare beryllium-copper surface. Figure 3-10 shows a circuit diagram of the important components of the floating probe sensor. *Siefring et al.* (1995) present a detailed description of each of these components and theory behind the measurement.

3.5   VEHICLE ENVIRONMENT.

Two of the most important parameters of the vehicle environment concerned with the HV vehicle - space interaction are the neutral gas density and the plasma density. Instruments to measure the ambient gas pressure close to the vehicle skin and also the ambient plasma density during the quiescent periods in the capacitor discharge program were included in the payload.

3.5.1   Neutral Pressure Gauge.

The pressure gauge used was a cold cathode ionization gauge similar to instruments flown on SPEAR-1 and SPEAR-2. The gauge was launched with a backfill of nitrogen and opened at altitude, thereby guaranteeing a fast start as the internal gauge pressure swept through the Paschen minimum. The access of gas to the ionization chamber was designed such that the time constant of the instrument to pressure changes was a few msec. Figure 3-11 is a schematic illustration of the magnetron sensor used within the neutral pressure gauge.

3.5.2   Langmuir Probe.

The Langmuir probe had cylindrical geometry, and the collecting area and a guard electrode were deployed a short distance from the vehicle skin. The probe was a gold plated cylinder with a length of 140 mm and a diameter of 2.4 mm. The bias to the probe consisted of a 0.9 sec fixed positive bias followed by a down/up sweep with a total duration of 0.1 sec. This ensured that the probe swept through the probe i-V characteristic at least once during the 1 sec quiescent periods enabling both T_e and the ion current to be measured during the undisturbed times during the flight. Figure 3-12 shows the mechanical configuration of the Langmuir probe.

3.6   VEHICLE RETURN CURRENT.

3.6.1   Skin Current Probes (SCP).

Two current collecting probes were set in the skin of the vehicle. Each probe was 74 x 165 mm in area and was fabricated and finished using the same material and surface treatment as the vehicle skin. One probe (SCP1) was mounted in the upper section of the payload and the other (SCP2) in the lower section, closer to the effluent releasing systems. Figure 3-13 presents a block diagram of the SCP1 electronics, and Figure 3-14 shows the mechanical assembly of SCP1.

3.7   EFFLUENT IONIZATION.

3.7.1   Optical Imaging Spectrometer.

A compact grating spectrograph with a total wavelength range of 1000Å and a spectral resolution of 5Å was coupled to a LLLTV camera which allowed both spectral and spatial resolution in two orthogonal directions in the camera image plane. The sensitivity of the camera's CCD (Charged Coupled Device) detector determined that the 1000Å range selected should fall within the overall range of 3500 - 8000Å. A 45° mirror deployed beyond the skin of the vehicle allowed the spectrometer to study optical emissions from the effluent gases from close to the skin out to about 3 m from the skin.

3.7.2   Low Light Level Televisions.

Two conventional white light imaging intensified LLLTV systems were also included in the payload. The cameras were each housed in a container pressurized to one atmosphere to protect the image intensifier from arcing. One of the units was pointed towards the graded boom to look for the presence of glow discharges around the grading rings and the biased sphere. The other camera was deployed far

enough away from the vehicle skin that an integral 45° mirror allowed a view parallel to the vehicle skin with a field-of-view including the complete solar cell system mounting plate after it had been deployed. The prime purpose of this camera was to record arcs on the biased solar cell arrays. However, the field of view was not completely filled by the arrays, and part of the region of effluent release was visible around the edges of the solar cell panel. The video signals from each camera were fed into a frame splitter, and the composite image was telemetered on a single TV downlink.

3.8   ARC MONITORS.

3.8.1   Transient Pulse Monitor.

The transient pulse monitor allowed the properties of impulsive signals to be characterized by peak positive and negative amplitudes, maximum rise and fall rates and the total time integral of the pulse signal. Three sensors were used to detect transient signals. A broadband current transformer monitored transient currents in any of the solar array samples. Transient longitudinal skin currents were measured at a slot machined into the payload skin. The third sensor used an active dipole/preamplifier to detect transient electric fields on the vehicle's surface.

3.9   HIGH SPEED DATA SYSTEM.

In order to measure the complete waveform of selected transient signals, a high-speed data system was included in the payload. The unit allowed the collection of data from a snapshot of 16 msec duration during which each of three channels were sampled at 1 MHz sampling rate. The initiation of the snapshot was controlled by a trigger signal, and provision was made to adjust the delay between receiving the trigger and starting the digitizing. This enabled the unit to be "tuned" to compensate for propagation delays in the systems being triggered. The three channels selected for high-speed sampling were the sphere to body potential, the sphere current through a Rogowski coil, and one of the skin current probes (SCP1). The synchronization was made to the initial application of the capacitor voltage to the sphere. Provision was made to read out the memories at a rate commensurate with the telemetry system capacity and the recharging time of the HV capacitors. Examples of the transient development of the current to the payload skin have been presented by *Thompson et al.* (1995).

3.10   PAYLOAD LAYOUT.

The instruments and support systems were packaged to fit into the 0.43 m diameter envelope of a Black Brant sounding rocket. The large number of instruments resulted in a very long payload which required extensive stress analysis to demonstrate that it would remain stable during the powered ascent to operational altitudes.

3.10.1   Longitudinal.

Figure 3-15 shows the arrangement of the different sections of the payload, and the instruments and support systems contained in the sections. The total length of the payload skin to the top of the HV section was 5.2 m, the telescopic boom supporting the sphere and graded boom was 2.0 m long, and the graded boom was 1.2 m long.

The sphere, graded boom and support boom were housed under the nosecone and deployed to the configuration shown in Figure 3-15 at nosecone release. The baseplate of the support boom housed the forward viewing LLLTV and the optical spectrometer and its deployment mechanism.

The high voltage originated in the high voltage section immediately below the nosecone and was conveyed to the sphere by a cable running up the support boom and inside the graded boom. The HV section was sealed and remained at a pressure of one atmosphere of dry air throughout the flight. It housed the HV power supply and capacitors, the HV switching relays and the HV monitoring sensors and signal conditioners.

Aft of the HV section was the first of the sections containing science instruments. The figure lists the instruments in that section which were, in general, either those needing to be further away from the effluent releasing devices or active devices which did not contribute to the effluent environment of the payload. The two electron emitting grounding devices were housed in this section.

The first science section was separated from the second by the vehicle service module. This section housed the support systems of power, telemetry and sequencing.

The second science section, aft of the vehicle service module, primarily housed the effluent releasing grounding devices and some instruments measuring the effect of the releases.

The final section of the payload, just ahead of the adapter ring to mate the payload to the rocket motor, was the attitude control system which provided control of the payload orientation in all three axes by releasing jets of cold nitrogen gas.

3.10.2 Azimuthal.

The azimuthal view, showing emission or deployment directions of the different instruments, is displayed in Figure 3-16. The figure is a view from the nosecone to the aft of the payload. Those instruments which view parallel to that direction have their look direction indicated by the dot and cross symbols indicating forward and aft directions respectively. The figure also indicates the direction of the geomagnetic field for the three orientations of the vehicle.

SECTION 4

INSTRUMENT CALIBRATIONS

Table 4-1. The SPEAR-3 instrument channels calibrations.

Signal	Description	Units	Min Value	Max Value	Resolution
SCSCUR1	Solar Cell #1 Current	μA	-11.03	9.01	0.07859
SCSCUR2	Solar Cell #2 Current	μA	-11.22	8.97	0.07919
SCSCUR3	Solar Cell #3 Current	μA	-10.88	8.96	0.07780
SCSCUR4	Solar Cell #4 Current	μA	-10.83	8.86	0.07722
ESAAH	ESA Low Gain/High Energy	eV	390	29000	7%
		$/E$-cm^2-ster-s	0	6.1×10^{13}	1.5×10^{10}
ESAAL	ESA Low Gain/Low Energy	eV	12	897	7%
		$/E$-cm^2-ster-s	0	6.1×10^{13}	1.5×10^{10}
ESABH	ESA High Gain/High Energy	eV	390	29000	7%
		$/E$-cm^2-ster-s	0	2.4×10^{11}	5.9×10^7
ESABL	ESA High Gain/Low Energy	eV	12	897	7%
		$/E$-cm^2-ster-s	0	2.4×10^{11}	5.9×10^7
DCDLIN	DCD Linear Voltage	V	-2510	2499	19.61
DCDLOG	DCD Log Voltage	V	-4385	11670	8.0%
TEACHTHIM	TE Cathode Current	mA	-22.22	227.8	0.9804
FEDGATEI	FED Gate Current	mA	-1.816	2.216	0.01581
FEDCATHI	FED Cathode Current	mA	-112.5	137.5	0.9804
RNGIM	Ring (Boom) Current	mA	-7.002	99.97	0.4195
DISIM	Capacitor Discharge Current	mA	-42.26	203.5	1.606
			203.5	1109	8.864
LOGSPHER	Sphere Voltage	kV	~ -200	~ 200	8.6%
LOGROG	Rowgowski Coil Current	A	~ -2000	~ 2000	15.3%
LPELEC	LP Electron Current	A	-3.0×10^{-9}	1.8×10^{-5}	6.2%
LPION	LP Ion Current	A	3.2×10^{-10}	1×10^{-3}	6.5%
NPNPM	Neutral Pressure	Torr	1.3×10^{-7}	8.3×10^{-4}	3.5%
PCRETNI	HCPC Neutralize Current	mA	0	560	2.196
SCP1CUR	SCP1 Linear Current	μA	-934.0	956.2	7.412
LOGSCP1	SCP1 Log Current	μA	-5025	8318	8.6%
SCP2CUR	SCP2 Linear Current	μA	-9693	10857	80
LOGSCP2	SCP2 Log Current	μA	-12740	10670	7.2%
FPHF21	FP High Frequency	V	-97	97	0.7608
FPV12M	FP Medium Gain 1	V	-193	194	1.520
FPV21H	FP High Gain	V	-24.2	24.2	0.1900
FPV12L	FP Low Gain	V	-1550	1550	12.16
FPV1S	FP Medium Gain 2	V	-710	115	3.235
TPMPAMP1	Electric Field Pos Amplitude	V/m	0	1.6×10^4	6.9%
TPMNAMP1	Electric Field Neg Amplitude	V/m	0	1.8×10^4	5.6%
TPMPDER1	Electric Field Pos Derivative	V/m-s	0	9.5×10^{12}	6.5%
TPMNDER1	Electric Field Neg Derivative	V/m-s	0	8.8×10^{12}	9.2%
TPMINT1	Electric Field Integral	V-s/m	0	3.3×10^{-2}	3.3%
TPMPAMP2	Bdot Pos Amplitude	A/m	0	7.5×10^1	4.4%
TPMNAMP2	Bdot Neg Amplitude	A/m	0	6.9×10^1	3.0%
TPMPDER2	Bdot Pos Derivative	A/m-s	0	7.5×10^9	6.9%
TPMNDER2	Bdot Neg Derivative	A/m-s	0	7.8×10^9	7.1%
TPMINT2	Bdot Integral	A-s/m	0	5.4×10^{-5}	3.7%
TPMPAMP3	SCS Pos Current Amplitude	A	0	7.4×10^0	3.8%
TPMNAMP3	SCS Neg Current Amplitude	A	0	7.0×10^0	3.8%
TPMPDER3	SCS Pos Current Derivative	A/s	0	9.3×10^8	
TPMNDER3	SCS Neg Current Derivative	A/s	0	9.4×10^8	9.4%
TPMINT3	SCS Current Integral	A-s	0	6.1×10^{-6}	4.3%

8

SECTION 5
BIASING TECHNIQUE

The biasing technique used was to connect a charged capacitor between a deployed sphere and the payload structure. To avoid electric field concentrations near the biased sphere support, the sphere was mounted on a boom containing grading rings which were interconnected by resistors, allowing a controlled fall off in the electric potential away from the sphere mount. Pre-flight calculations showed that the system geometry, combined with expected ionospheric plasma densities, required a capacitor bias of 10 kV to bias the payload to at least -2 kV relative to the ionosphere at operational altitudes. A capacitor was chosen as the prime source of bias potential because it would be able to sustain high currents if external discharges occurred, moreover as the capacitor discharged through fixed resistors and the ionospheric plasma, the bias voltage would sweep through a range of values. A 2 μF capacitor was chosen to allow a time constant commensurate with the telemetry sampling intervals, maximizing the number of capacitor discharges for the flight time. The latter requirement was aided by using two capacitors such that one was being charged while the other was in its discharge cycle. The current from the capacitors was limited to 5 amps by a 2 kΩ resistor in series with the capacitor. Figure 5-1 shows a simplified schematic diagram of the biasing technique and the relative locations of the sphere to the payload and to the payload voltage monitoring instruments.

It was decided that two modes of HV connection to the sphere would be used. One allowed the voltage to rise as rapidly as it could following the closure of a HV relay between the sphere and the charged capacitor - this was called the switched mode. The other mode interposed a resistor/capacitor network between the relay and the sphere to slow down the rise in potential such that it took about 30 msec to reach its peak value - this was called the ramped mode. Simplified schematics of the two biasing schemes are shown in Figure 5-2. The parallel combination of the fixed 700 kΩ resistors and the 1 MΩ resistance built into the graded boom set the decay time constant of the 2 μF capacitor to be 0.82 sec in the absence of external plasma. In the ramped mode, the 30 kΩ resistor in the delay circuit and the charge shared with the 0.5 μF capacitor reduced the peak voltage between the sphere and the payload from the initial voltage across the 2 μF capacitor of 10 kV to ~8 kV. Figure 5-2 also shows the electrical configuration of the sphere and the payload during the one second passive period which followed each four second discharge period.

9

SECTION 6
MISSION OPERATIONS

6.1   LAUNCH.

The payload was launched from the NASA range at Wallops Island, Virginia, at 21:12:41 EST on March 15, 1993 in an easterly direction. A digisonde ionospheric sounder located near the range determined the peak ionospheric plasma density to be ~3 • 10^{11} m^{-3} with the altitude of the F-region peak at 340 km, considerably above the apogee altitude. The launch time was within the window required for darkness at apogee.

6.2   TRAJECTORY.

The trajectory of the payload reached an apogee of 289 km 278 sec after launch. This was under the goal of 300 km but was close enough to provide time to exercise all of the planned modes before the payload ceased functioning upon re-entry. The azimuth of the trajectory was ~100°.

6.3   ATTITUDE MANEUVERS.

Three science-related attitude maneuvers were made during the flight. Figure 6-1 shows the times of the maneuvers and a diagrammatic sketch of the payload orientations after each maneuver. The first position resulted in the payload longitudinal axis and the axes of symmetry of the four gas release system plumes being perpendicular to the geomagnetic field. The second maneuver rolled the payload 90° about its longitudinal axis to orient the gas release system plumes to be parallel to the geomagnetic field, but still keeping the geomagnetic field perpendicular to the payload axis. In both of these attitudes the maximum magnetic insulation was achieved between the biased sphere and the payload skin and effluent release devices.

The final attitude placed the geomagnetic field parallel to the payload axis. This provided a situation where there was the greatest possibility for reduced impedance between the sphere and the payload because of the low impedance to plasma currents parallel to magnetic fields.

SECTION 7

FLIGHT OBSERVATION PROGRAM

The flight observation program consisted of cycling through the four grounding devices interspersed with periods when no planned grounding was initiated. The high voltage biasing was initiated at an altitude of 150 km about 100 sec after lift-off.

In each sequence, the grounding device to be tested was active for a total of four discharges of the biasing capacitors. The first pair tested the effectiveness of the grounding device for a ramped and a switched application of the bias. Also, when feasible, the grounding device was activated about 100 msec prior to the capacitor discharge for each of the two switching modes. The second pair of biasing capacitor discharges with the selected grounding device again tested the ramped and switched modes, but in this case the grounding device was activated about 100 msec after the capacitor discharge. Thus the exercise of a given grounding device occupied four capacitor discharge cycles, a total of 20 sec.

The order of using the grounding devices and their distribution in altitude and attitude is shown in Figure 7-1 where letters signifying the device used are plotted on an altitude trajectory. The periods of time when the ACS was used to re-orient the payload are shown by the gray bars.

High-speed data snapshots of the three channels described earlier were taken for the first 16 msec of each of the capacitor discharges.

SECTION 8

RESULTS

8.1 INSTRUMENT FLIGHT PERFORMANCE.

The majority of the instruments and support sub-systems worked well during the flight. All of the mechanical functions performed as expected and at the planned times. All prime power systems worked correctly and maintained adequate bus voltages throughout the flight.

The support system which failed was one of the TV telemetry transmitters. The transmitter performed well through all of the powered flight, and video images from the two cameras it was supporting were as expected. At about 70 sec into the flight the telemetry signal was lost and never re-appeared.

Two of the instruments appeared to suffer some malfunction. The hollow cathode plasma contactor did not produce the expected emission current and was unable to provide the grounding function expected. It is suspected that the cathode was poisoned prior to lift-off during the short period it was exposed to the payload purge gas. The field emission device was believed to have lost some of its nine modules when it was initially activated. This was thought to be a consequence of contamination around the payload which had not reduced sufficiently at the first activation time. However, although this reduced its current capacity, there was enough current to discharge the vehicle at lower ionospheric plasma densities.

The attitude control system worked well and re-oriented the payload to the required positions at the planned times. Since these attitude changes were planned to occur during times when the payload was biased, the ACS provided an alternate gas release grounding system.

8.2 BIASING ACHIEVED.

The biasing program consisted of alternating the ramped and switched modes of sphere bias throughout the flight. After 4 secs of connection time for the capacitor to the sphere, the sphere was grounded by another HV relay for a period of one second. This operation provided one second of quiescent data each capacitor discharge, and also drained any residual charge from the biasing capacitor before it started its next charging cycle.

Figure 8-1 shows the simplified schematic including the external plasma impedances between the sphere and payload to the undisturbed ionosphere. Under normal circumstances these two impedances are large compared with other circuit impedances. However, in the event of and external discharge at either the sphere, the payload or both, these impedances become small and influence the attainment of the desired potentials because of the current limiting provided by the 2 kΩ resistor in series with the biasing capacitor. Reduced plasma impedance also increased the rate of decay of the potential between the sphere and the payload.

The effect of external discharge was seen early in the SPEAR-3 flight. Figure 8-2 shows the measured sphere to payload potential for the ramped mode followed by the switched mode at two times during the flight. At the earlier time neither capacitor discharge reaches its expected potential, and the switched mode achieves a lower potential than the ramped mode. This is interpreted as an external discharge triggered at sphere bias initiation, and occurring at a lower threshold for the switched case than for the ramped case. At the later flight time the sphere potentials are seen to behave as expected. This effect has been studied in more detail and related to payload outgassing (*Raitt et al.,* 1995b).

8.3 GROUNDING EFFECTIVENESS.

8.3.1 Neutral Gas Release System (NGRS).

An example of payload grounding achieved by the neutral gas release system is shown in Figure 8-3. The figure shows a plot of several parameters against mission elapsed time (time from launch) for the duration of one biasing capacitor cycle when the neutral gas release system was operated in the mode of being activated after the HV bias was applied. The top bars show the capacitor discharge on when the line is thick, followed by the times when the high gas flow valves are open, then the times when the low gas flow rate valves are open. The first high flow period lasts for 200 msec while the subsequent ones

12

have a duration of 100 msec. The upper plot panel shows the regulator pressure responding to the valve openings, and the lower panel shows the payload potential measured by the floating probe.

The plot shows that the payload potential falls to a negative voltage beyond the range of the floating probe channel used as soon as the biasing capacitor is connected. When the high flow rate gas emission is initiated, the payload potential immediately drops to ~ -230V. The return to a high negative potential is slow and is stopped by the low flow rate gas emission. After remaining low for a period exceeding the gas flow period, the potential eventually jumps back to a high negative potential but is brought down again by the next high flow rate period. Finally, after 306.5 sec the biasing capacitor has discharged to a level that the payload is no longer at a high enough bias to allow the gas released to be ionized, and there is no more grounding by the system. This effect has been compared with other sound rocket payloads by *Berg et al.* (1995).

This behavior is typical of that seen throughout the flight. The most apparent anomalous result seen is the delay in the return of the payload to high negative potential after the gas flow is shown as having stopped.

8.3.2 Hollow Cathode Plasma Contactor.

We believe that the hollow cathode plasma contactor suffered a cathode failure as discussed earlier, so it was unable to perform its grounding function as planned. Figure 8-4 shows a capacitor discharge period when the hollow cathode plasma contactor was activated. The top bars show the capacitor discharge period, and below it the enable command for the hollow cathode plasma contactor. The upper plot panel shows evidence of the electrical functioning of the system where the keeper voltage is plotted. The lower panel shows the payload potential measured by the floating probe. It can be seen that the payload potential is just changing in a way which tracks the exponential decay of potential on the biasing capacitor. There is some evidence that the time constant is reduced, which may be due to ionization of the gas emitted by the device at a low flow rate.

8.3.3 Thermionic Emitter.

The thermionic emitter was activated by applying power to heat the filament to emission temperatures. An example of the grounding achieved with this device is shown in Figure 8-5. The top two bars showing the biasing cycle and the filament activation indicate that this was a case where the grounding was initiated after the bias had been established. In the case of this device, the grounding was not immediate since the filament took about 200 msec to reach emission temperature as is shown by the rise in the cathode current. The lower plot panel shows the floating probe measure of payload potential which is reduced from a high negative value to ~ -100V when the electron emission occurs. The payload potential then decays at an accelerated rate until reaching plasma potential. During an earlier grounding sequence, the TE charged the vehicle a few volts positive

During the course of the flight we found that effective grounding of the payload only happened at positions in the trajectory where the ambient plasma density was low. We believe that this is due to the low perveance of the electron emitter which cannot supply enough current to balance that collected by the biased sphere at higher plasma densities.

8.3.4 Field Emission Device.

The behavior of the field emission device was similar to the thermionic emitter. Figure 8-6 shows a plot of parameters associated with the field emission device and the response of the payload potential measured by the floating probe.

The upper bars show the biasing cycle and the field emission device activation. The device was activated after biasing was established, but like the thermionic emitter there is a further delay before it is capable of emitting electrons. In this case the delay is a controlled ramp up of the gate potential over a period of one second to reduce the risk of tip arcs. The upper panel shows the total current emitted by the devices reflecting the ramp up of the extraction potential. The lower panel shows that the payload potential initially falls to a high negative value on the application of the bias. This is followed by an attempt to return to low values when the field emission device ramp-up starts, but this is a transient event, and the grounding does not occur until the full emission current is established. The payload potential is then brought to ~ -200V and remains low for the rest of the capacitor discharge cycle.

13

The flight history of the effectiveness of the field emission device to ground the payload was similar to the thermionic emitter. The perveance of this device is also low and the current delivered does not appear to be sufficient to cope with the collected current at high ionospheric plasma densities.

8.4   VEHICLE ENVIRONMENT.

8.4.1   Neutral Pressure Gauge (NPG).

The NPG functioned well throughout flight. Figure 8-7 compares the pressure measurements made by the NPG with two models: the model represented by the solid line is the MSIS-86 model atmosphere for the time of flight (*Hedin,* 1987), and the model represented by the dashed line is what the NPG would measure in the MSIS-86 model atmosphere based on the vehicle velocity. The NPG measurement exceeded the model throughout flight, merging on reentry. The elevation in pressure is presumed to result from outgassing of the payload. The SPEAR-1 pressure measurement exhibited a similar profile.

Also evident in the NPG measurement are pressure enhancements associated with gas releases. The larger enhancements correspond to releases by the NGRS, and the smaller enhancements correspond to ACS jet firings. On closer inspection it is observed that the roll jets caused much larger enhancements than the pitch/yaw jets and that, of the pitch/yaw jets, only the one directly below the NPG caused any perceptible enhancements. These observations suggest that collisions with the vehicle play an important role in scattering the neutral gas into the NPG.

8.4.2   Langmuir Probe.

During most periods when no grounding devices were operating and the high-voltage sphere was shorted to the rocket body, the current characteristics of the Langmuir probe were close enough to classical curves to compute estimates of the electron density and temperature. Figure 8-8 plots estimates of the electron density, and Figure 8-9 plots estimates of the electron temperature. The electron density estimate appears to be quite reliable, and, at apogee, it agrees well with the density measured by the Wallops ionosonde. The electron temperature estimate in Figure 8-9 does not appear to be as reliable, being widely scattered between 500 and 1000 K, showing a tendency to peak near 200 km. A realistic temperature profile would be expected to increase monotonically at these altitudes.

A piecewise polynomial curve fit of the electron density deduced from the Langmuir probe data has been incorporated into the on-line SPEAR-3 database at Utah State University.

SECTION 9
CONCLUSIONS

The SPEAR-3 experiment performed well during its flight with the following exceptions:

(i)   One TV telemetry link failed ~70 sec after lift-off

(ii)   The hollow cathode plasma contactor current was low

(iii)   There appeared to be a failure of some FED modules at initial switch-on

The grounding devices worked with varying degrees of effectiveness at different altitudes, which appears to be related to their current carrying capability to match the electron current collected by the positively biased sphere. In summary:

(i)   The neutral gas release provided consistent grounding at all operational altitudes to a payload potential of ~ -230V using an 8g/sec flow rate.

(ii)   The hollow cathode plasma contactor was unable to achieve grounding of the payload due to low emission current believed to have been caused by a poisoned hollow cathode.

(iii)   The thermionic emitter was most effective at lower altitudes when the ionospheric plasma density was low and the emission current could match the sphere current.

(iv)   The field emission device was found to be more effective later in the flight, again when the ionospheric plasma density was low. The low plasma density ascent data was affected by suspected module arcing when the payload was still outgassing heavily.

Early application of HV bias to the system showed evidence of local breakdown during the heavy outgassing period which prevented the full bias voltages from being achieved. This differed from the SPEAR-1 experience but is consistent with the much later, higher altitude of the initiation of biasing on the SPEAR-1 flight. SPEAR-1 did show a similar breakdown late in the flight upon re-entry.

SPEAR-3 provided much valuable data on grounding devices and the associated HV-space environment interaction. Together with the SPEAR-1 data this provides a good indicator of these effects from a slow moving space platform. The next major advance in this area of study will come from the measurement of HV-environment interactions from orbital platforms. The transition from subsonic to supersonic (for ions) has a significant effect on ion collection, and new experimental data needs to be taken. Also the initial outgassing of sounding rockets due to their short exposure to the upper atmosphere clearly has a significant influence on the HV interaction.

The generation of the HV for biasing can conveniently be developed on orbital platforms by the use of electrodynamic tethers. We hope to see more experiments beyond those currently planned in this area in the next few years. Finally, the practical applications of the results of HV interaction studies are primarily going to be applied to orbiting systems, so it is time to move into this domain with our experiments.

SECTION 10
REFERENCES

Berg, G. A., W. J. Raitt, D. C. Thompson, B. E. Gilchrist, N. B. Myers, P. Rodriquez, C. L. Siefring, H. R. Anderson, D. W. Potter, Overview of the effects of neutral gas releases on high-voltage sounding rocket platforms, *Advances in Space Research, 15*, 12, (12)83-(12)86, 1995.(U)

Hedin, A. E., MSIS-86 Thermospheric model, *J. Geophys. Res., 92*, 4649, 1987.(U)

Raitt, W. J., G. Berg, D. Thompson, A. B. White, B. Peterson, M. Roosta, M. Jensen, L. Allen, J. Antoniades, P. Rodriguez, C. Siefring, H. Anderson, D. Potter, J. Jost, R. Adamo, D. Dana, C. Holland, J. Pickett, R. Merlino, M. Adrian, N. Grier, N. Poirier and R. Morin, SPEAR-3: A sounding rocket experiment to study methods of electrically discharging a negatively charged space platform at LEO altitudes, J. Spacecrafts and Rockets, 1995a.(U)

W. J. Raitt, G. A. Berg, D. C. Thompson and S. Sazykin, Measurements of electrical breakdown in the vicinity of a sounding rocket differentially charged to 10 kV, *Advances in Space Research, 15*, 12, (12)79-(12)82, 1995b.(U)

Siefring, C. L., P. Rodriguez, M. M. Baumback, J. A. Antoniades, and D. N. Walker, A method for measuring large changes in the payload voltage of rockets and satellites, submitted to *Reviews of Scientific Instruments*, 1995.(U)

Thompson, D. C., W. J. Raitt, G. A. Berg, Transient measurements of HV interaction with the ambient and perturbed space environment, *Advances in Space Research, 15*, 12, (12)91-(12(94), 1995.(U)
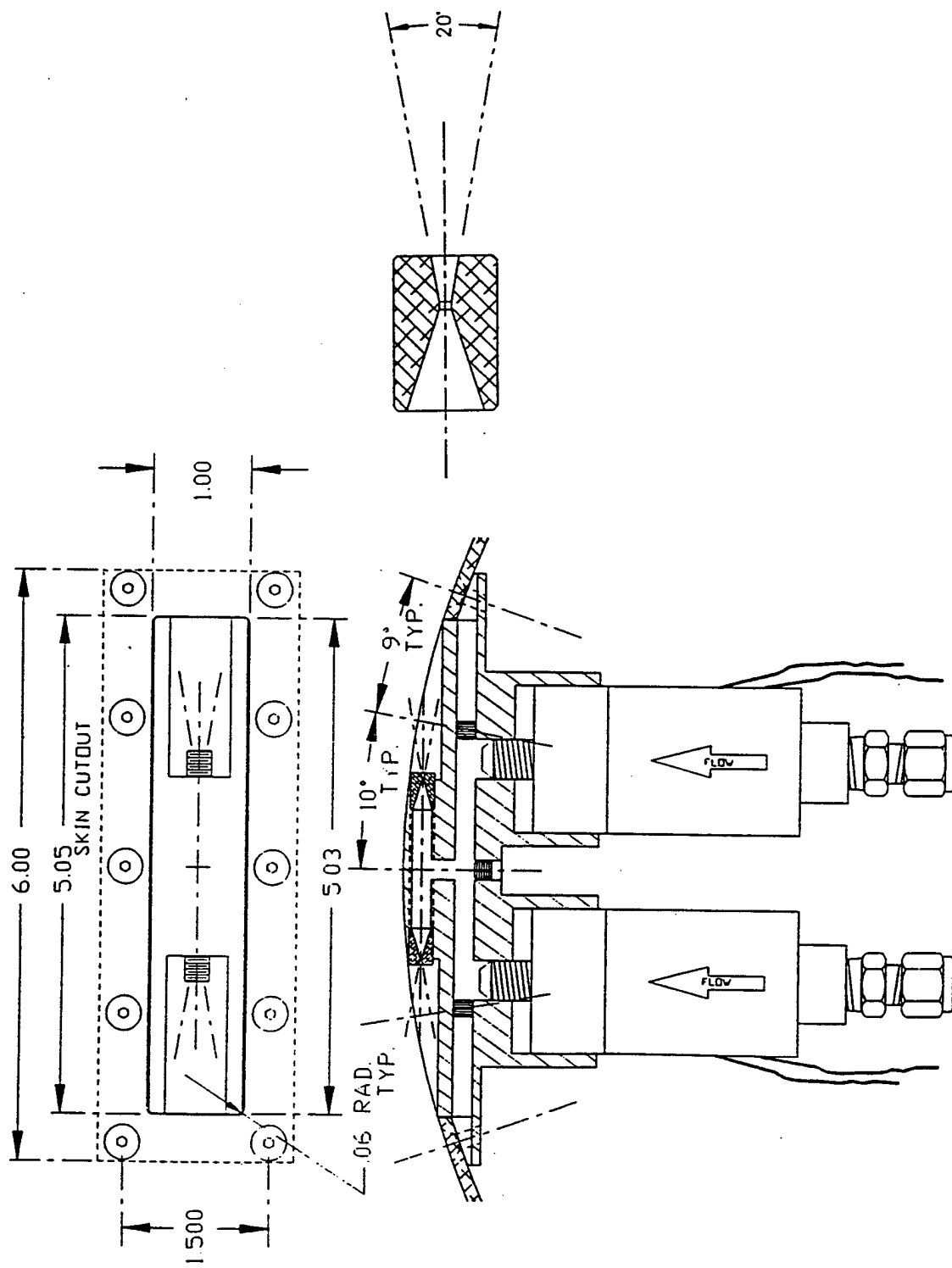
Figure 3-1. Assembly drawing of a nozzle block from the neutral gas release system and an enlarged view of a single screw-in nozzle.

17

HCPC ASSEMBLY DRAWING

PART NO	DESCRIPTION	QTY
16		1
15		
14		
13	TERMINAL	9
12	WASHER #2	6
11	SCREW 2-56x1/2	3
10	SS-200-R-4	SCREW 2-56x1/4	1
9	SS-400-61	REDUCER	1
8	SS-400-R-4	BULKHEAD UNION	1
7		REDUCER	3
6		INSULATOR SUPPORT	3
5		KEEPER SUPPORT	2
4		CONNECTOR	1
3		BASE PLATE	1
2		INSULATOR	
1	400021	KEEPER PLATE	
		CATHODE	

SYSTEM PLANNING CORPORATION
CENTER FOR SPACE PHYSICS
SUITE 308, 18100 UPPER BAY ROAD
HOUSTON, TEXAS 77058 (713) 333-2644

CATHODE ASSY.

Figure 3-2. Assembly drawing of the cathode for the hollow cathode plasma contactor.

THERMIONIC EMITTER FILAMENT ASSEMBLY

(Semicon Part #LRF003)

3X Ø.120/.124
∨ Ø.230
⊕ Ø.004 A B

Ø1.320

3X 120°

Ø1.565±.002

-B-

.529

.070

.525±.002
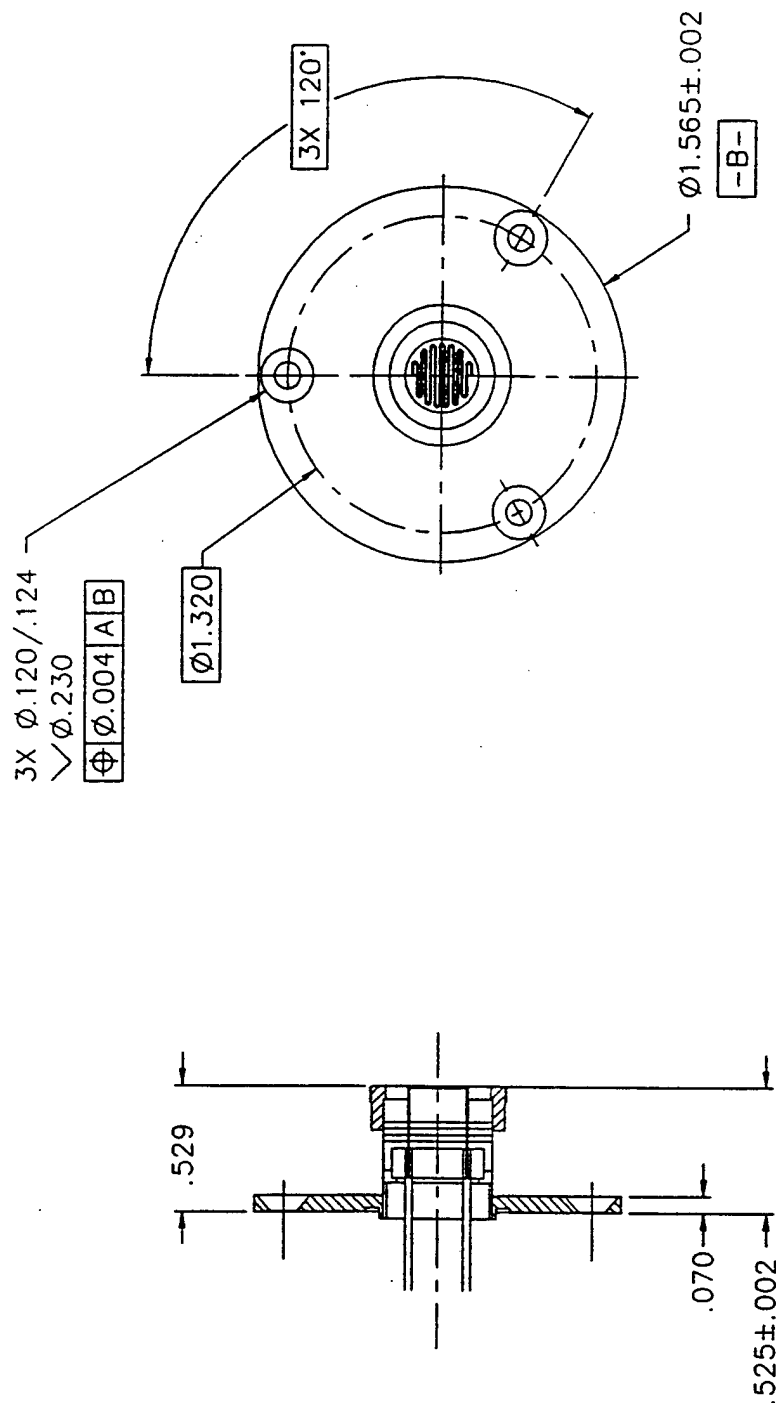
△ .660 NOMINAL ±.03 ADJUSTMENT

Figure 3-3. Assembly drawing of the thermionic emitter filament.

METAL
TIPS

METAL GATE
FILM

1 μm

SiO$_2$ DIELECTRIC

~3/4 μm

SILICON BASE

sp-012694-jd
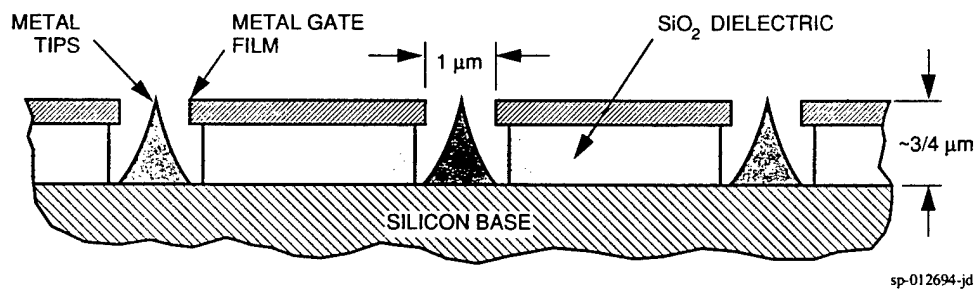
(a) SCHEMATIC OF A SPINDT CATHODE ARRAY

10 μm
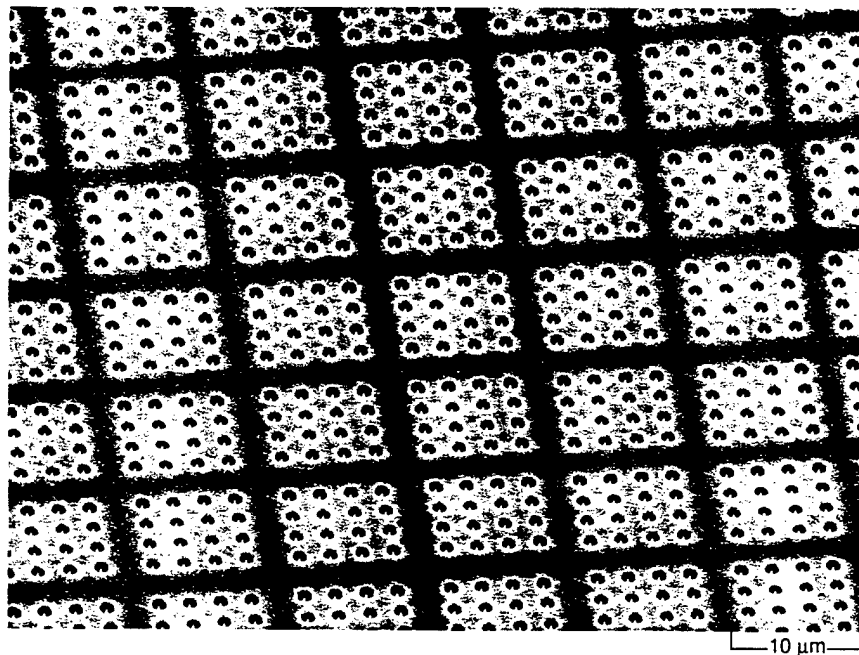
(b) SEM MICROGRAPH OF SPINDT CATHODE ARRAY

1 μm
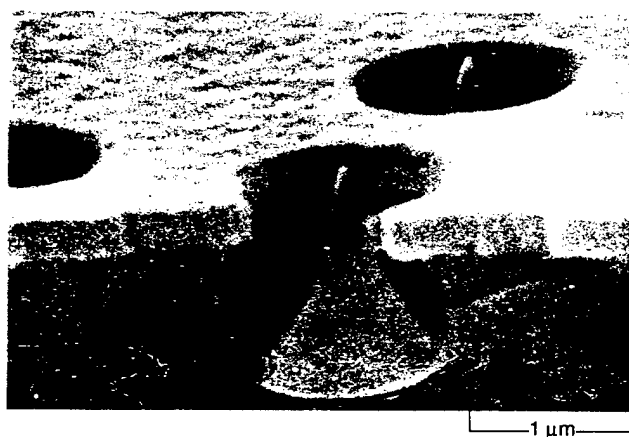
(c) SEM MICROGRAPH OF SPINDT CATHODE

Figure 3-4. (a) Schematic illustration of enlarged view of an FED array. (b) Micrograph of
a region from an FED array. (c) Micrograph of a single FED cathode.

20

DIFFERENTIAL CHARGE DEVICE BLOCK DIAGRAM
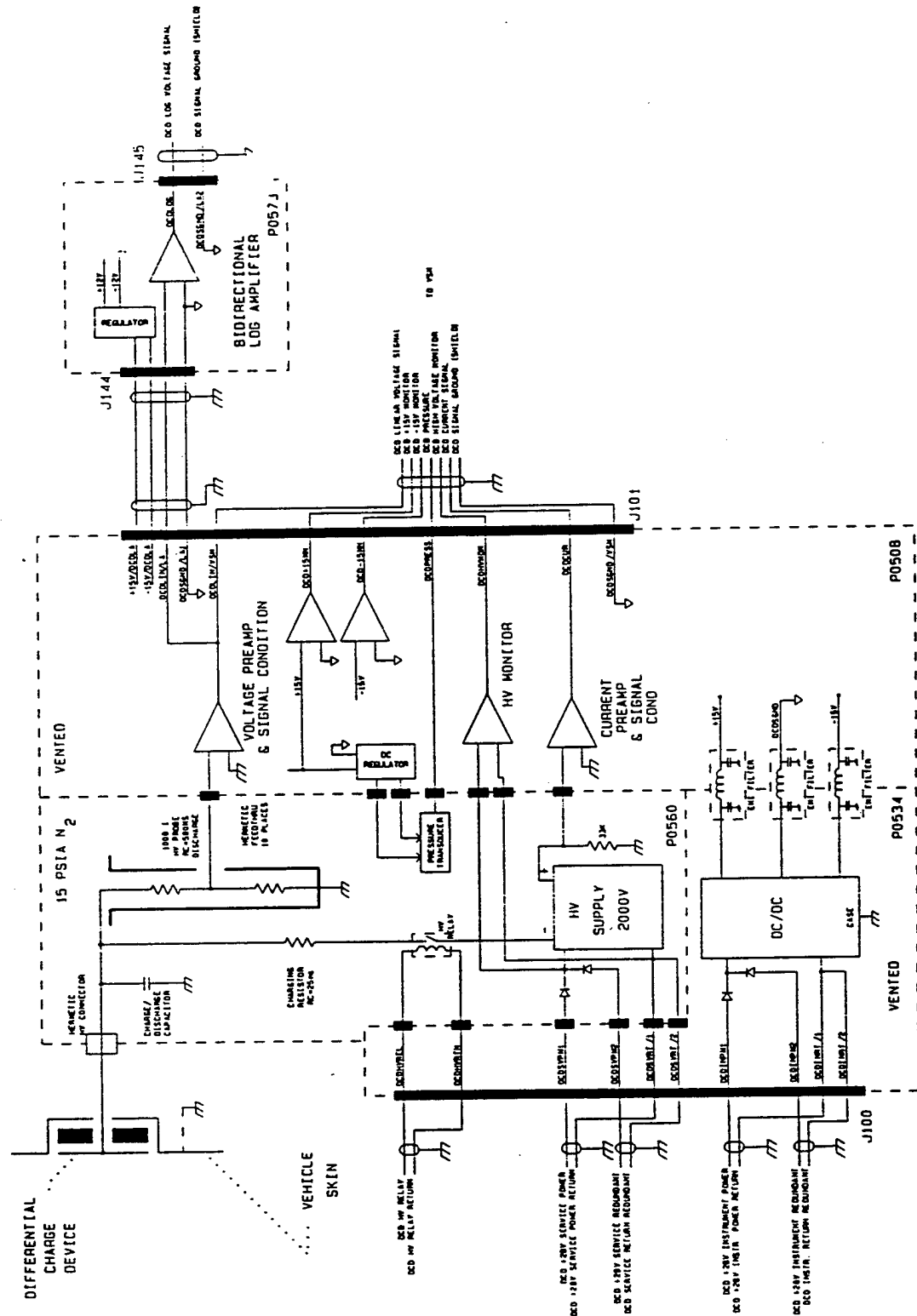
Figure 3-5. Electrical block diagram of the differential charge device.

DIFFERENTIAL CHARGING DEVICE

8.63

4.50

3.44

8.00

6.94

4.88
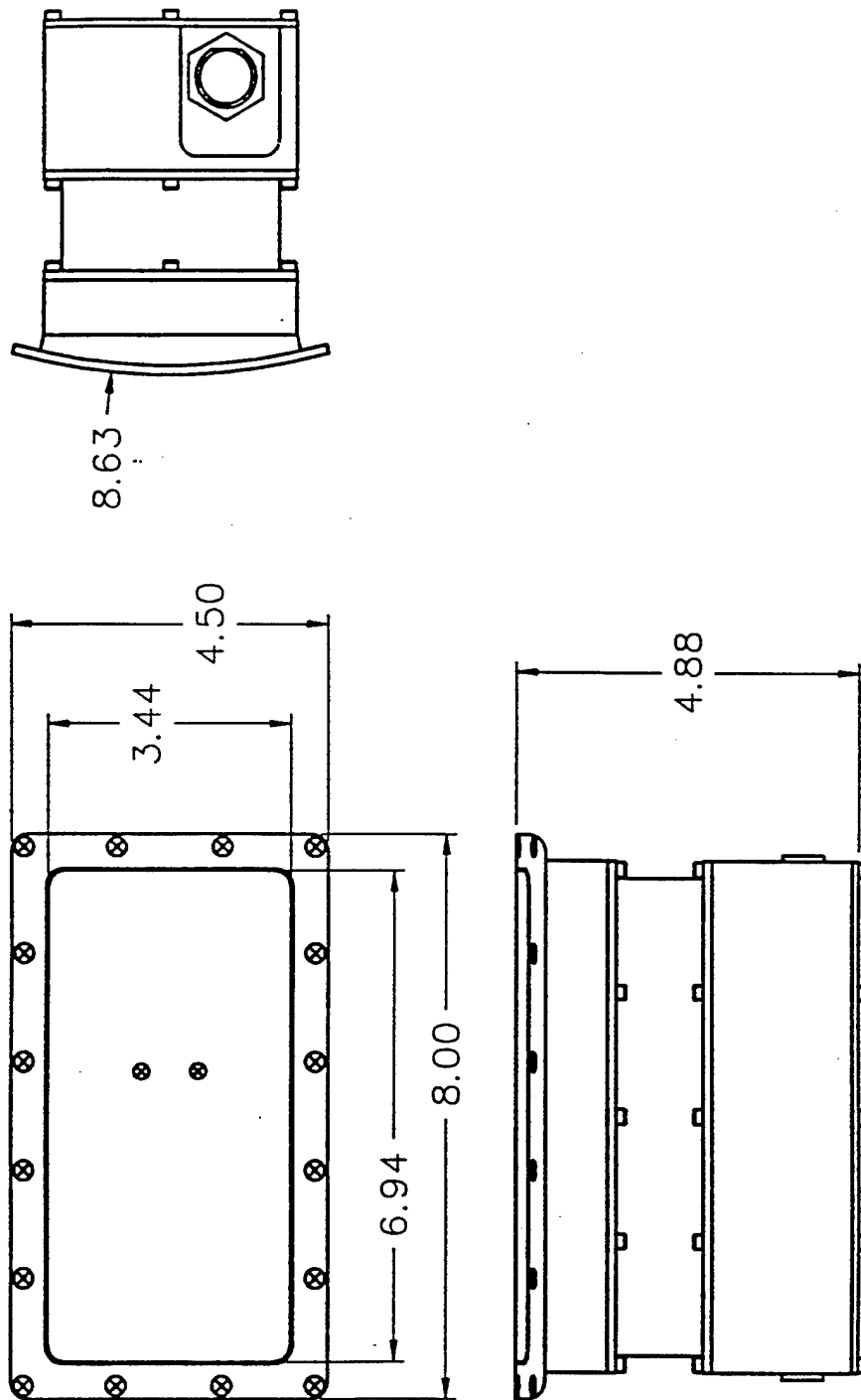
Figure 3-6. Assembly drawing of the differential charge device.

22
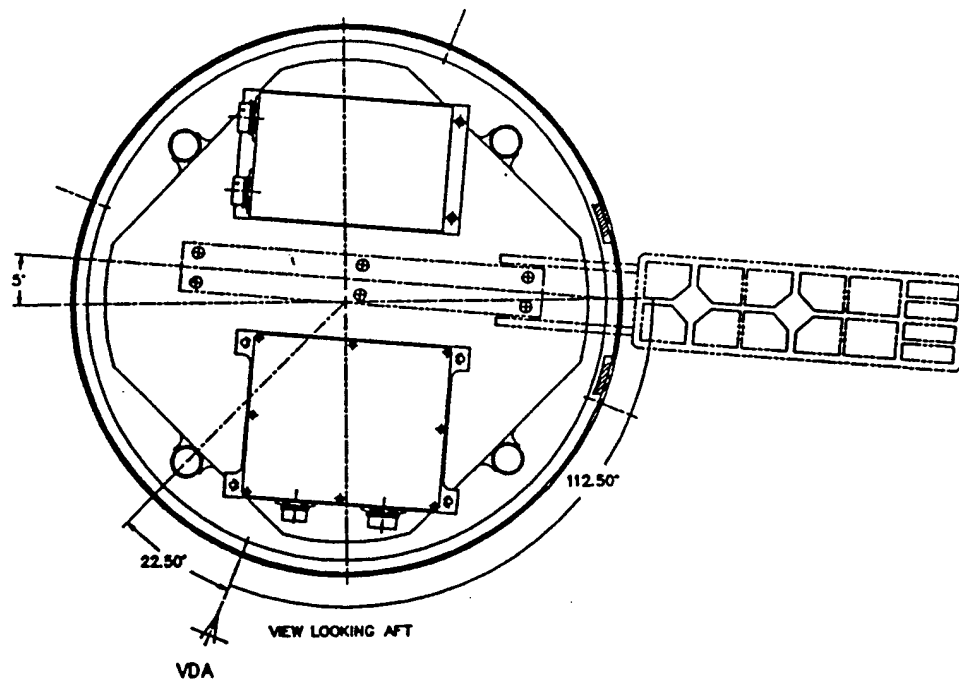
Figure 3-7. Deployed position of the solar cell system.

23
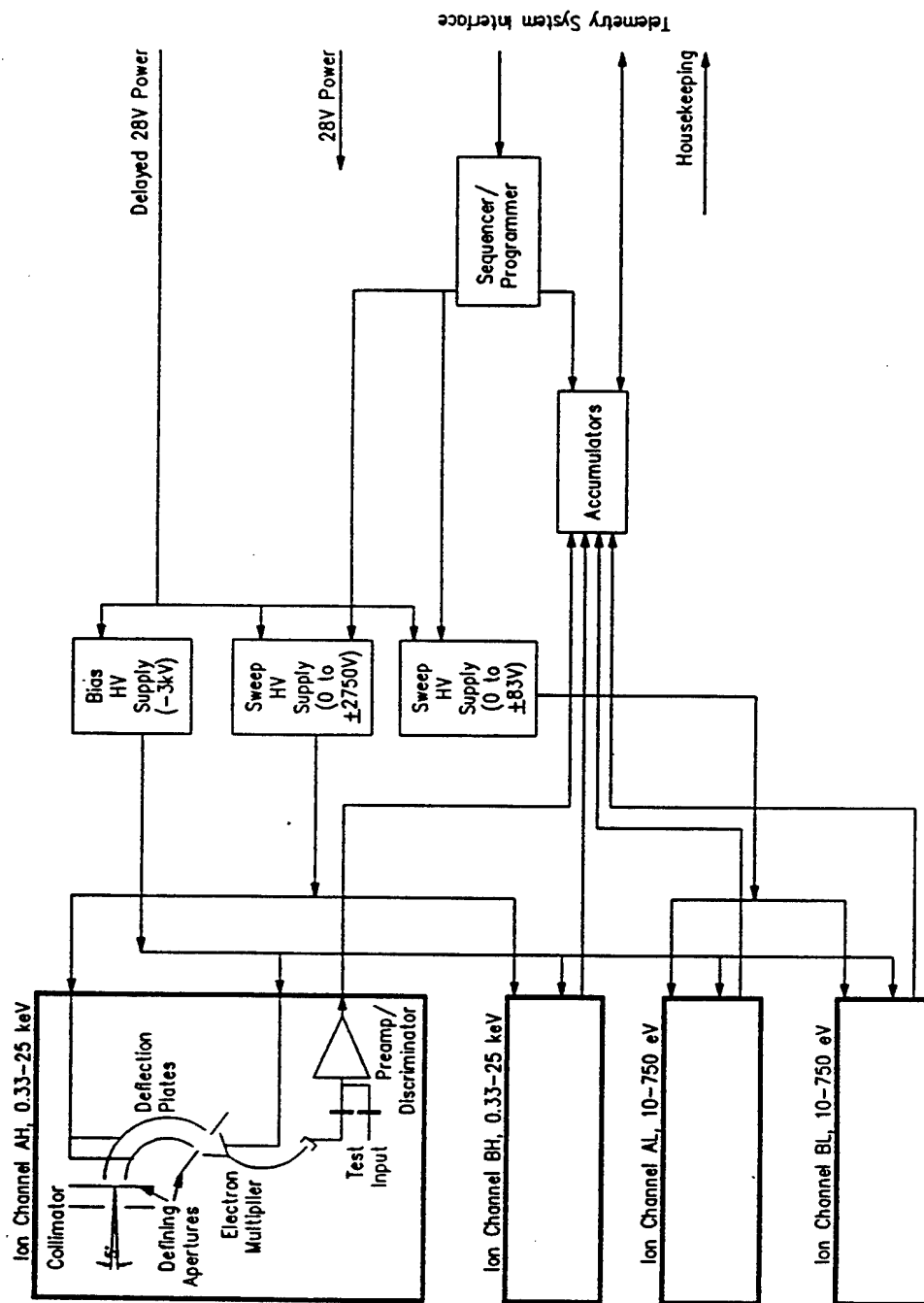
Figure 3-8. Block diagram of the electrostatic analyzer.

24
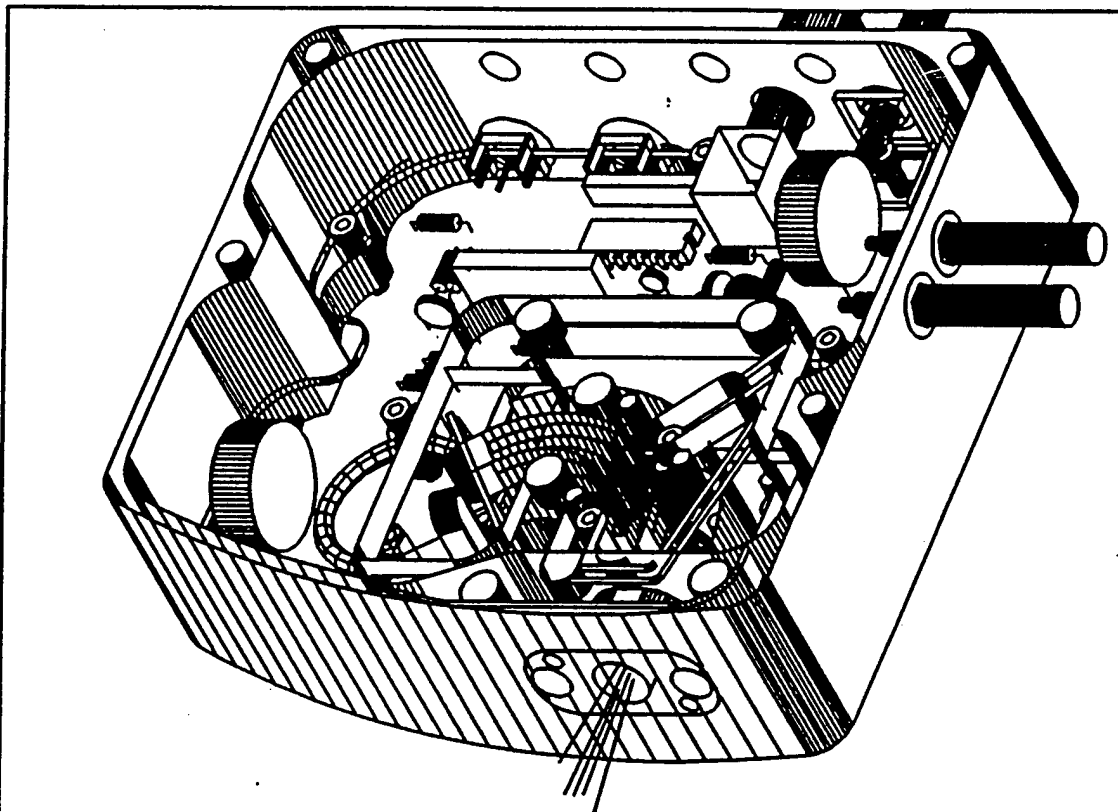
CPD Sensor — Conventional 127° Cylindrical
Curved Plate Analyzer with Channeltron Detector.

Figure 3-9. Drawing of an assembled ESA sensor.

25

Floating Probe
Spherical Sensor
2.5" (6.35 cm) Diameter
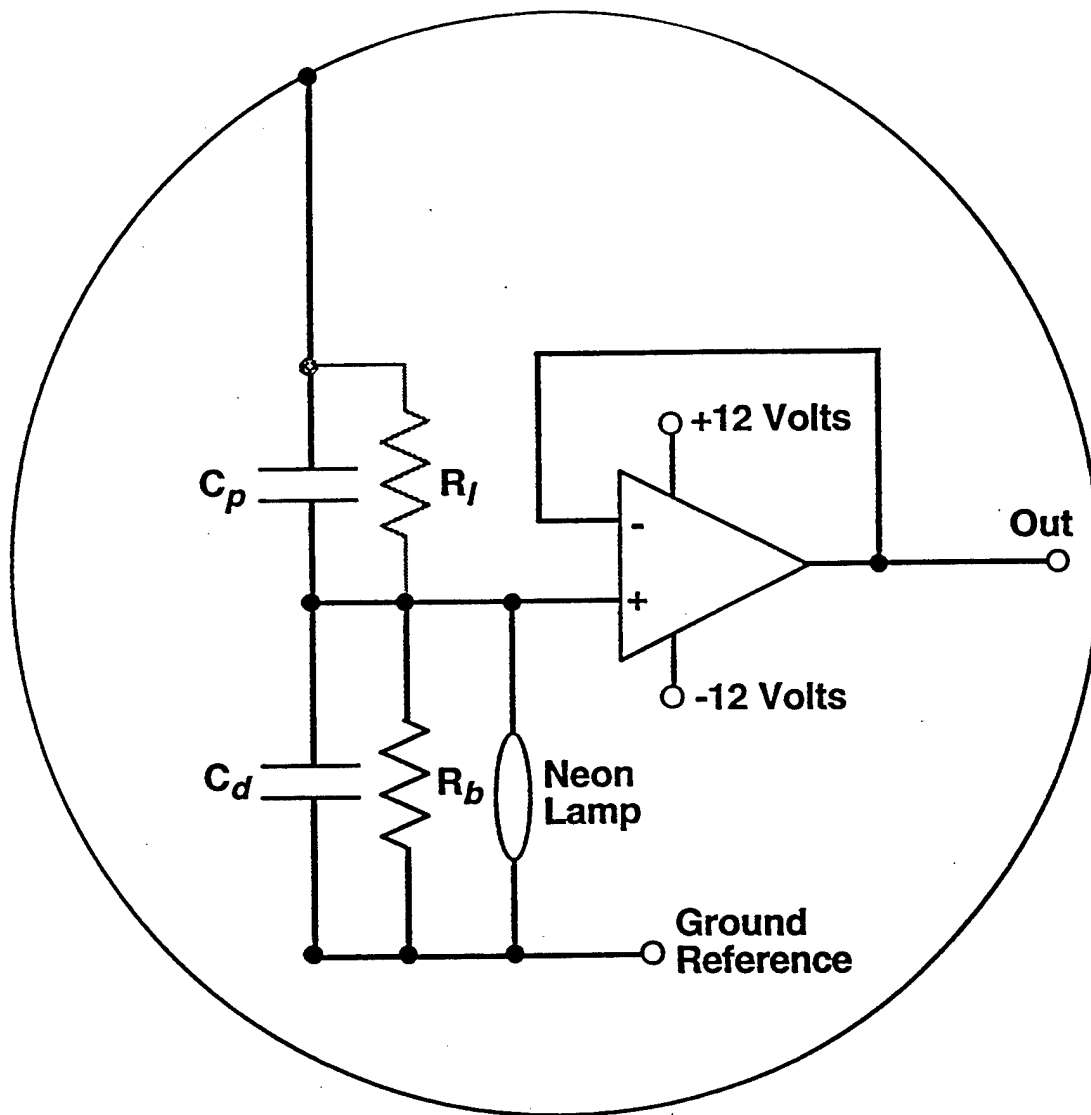
Figure 3-10.   Circuit diagram of the floating probe sensor.

B

Anode Shell

Cathode

Insulating Teflon Sleeve

Ceramic Insulator
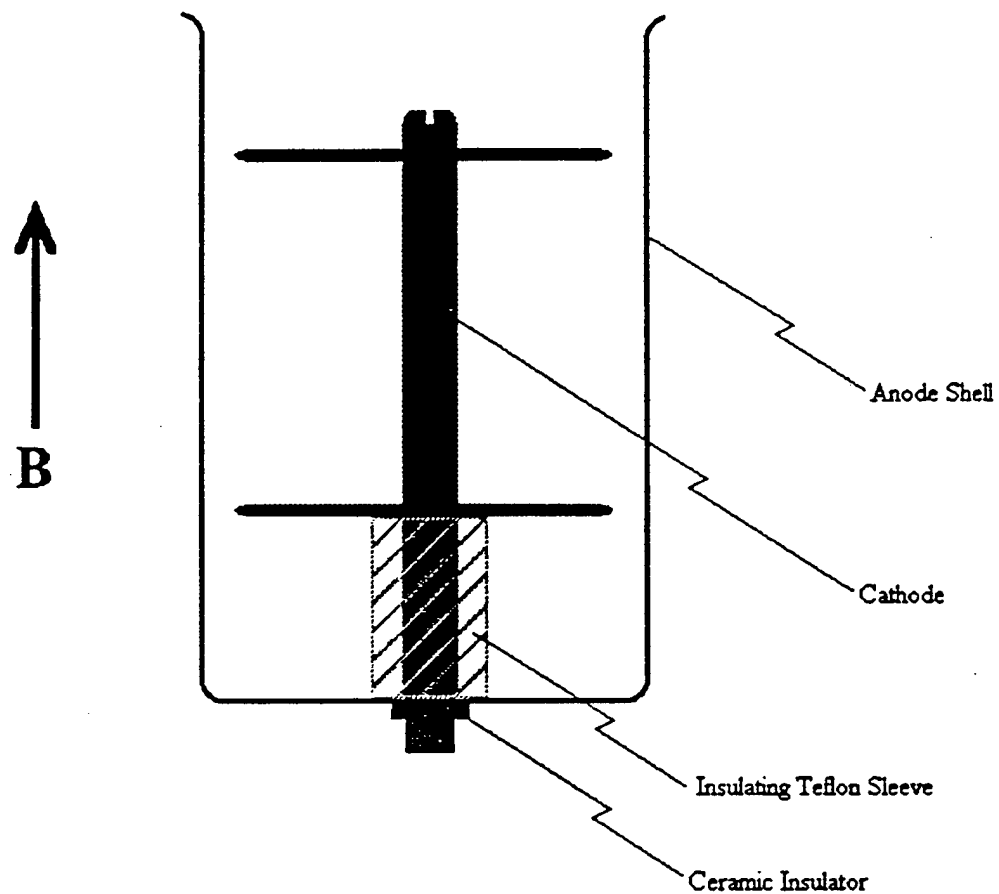
Figure 3-11.   Schematic drawing of the magnetron sensor used in the neutral pressure gauge.

Figure 3-12. Assembly drawing of the Langmuir probe electrode configuration.
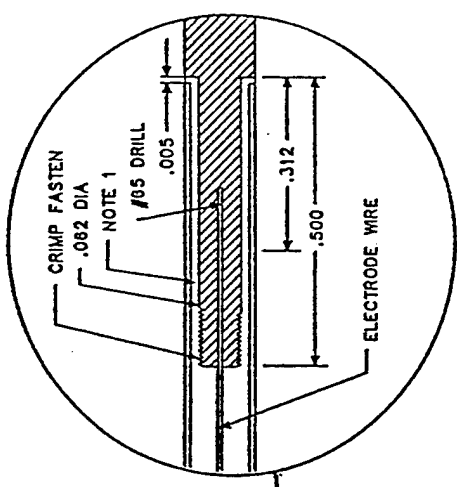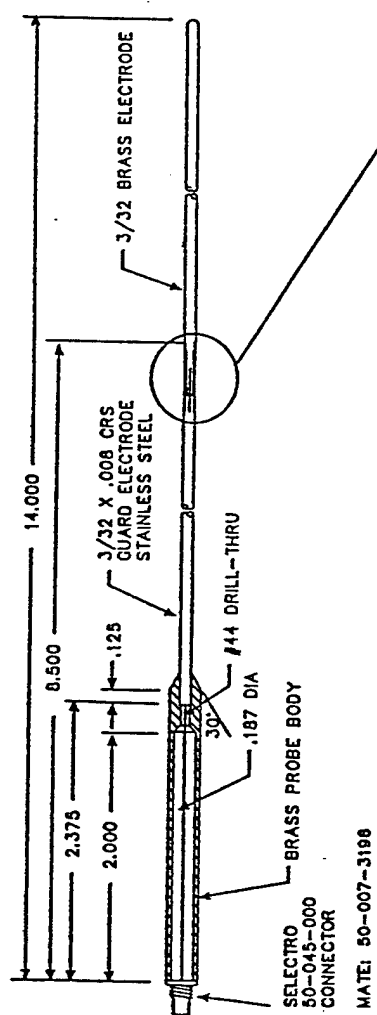
NOTE:
1. MACHINED EPOXY INSULATOR
2. COATING FOR SPEAR I and II: PAINT WITH AERODAG G
3. COATING FOR SPEAR III: NICKLE STRIKE AND GOLD PLATE
   AS PER MIL SPEC MIL-G-45204 TYPE 2, CLASS 1 (50μ INCHES)

CRIMP FASTEN
.082 DIA
NOTE 1
#05 DRILL
.005
.312
.500
ELECTRODE WIRE

3/32 BRASS ELECTRODE

3/32 X .008 CRS
GUARD ELECTRODE
STAINLESS STEEL

#44 DRILL-THRU

.187 DIA
30°

BRASS PROBE BODY

SELECTRO
50-045-000
CONNECTOR

MATE: 50-007-3198

14.000
8.500
2.375
2.000
.125

SPACE DYNAMICS LABORATORY
UTAH STATE UNIVERSITY
LOGAN, UTAH 84322-4140
(801) 750-2905

TITLE
LANGMUIR PROBE ELECTRODE CONFIGURATION

DRAWING NUMBER
B4-3738

28

SKIN CURRENT PROBE #1 BLOCK DIAGRAM
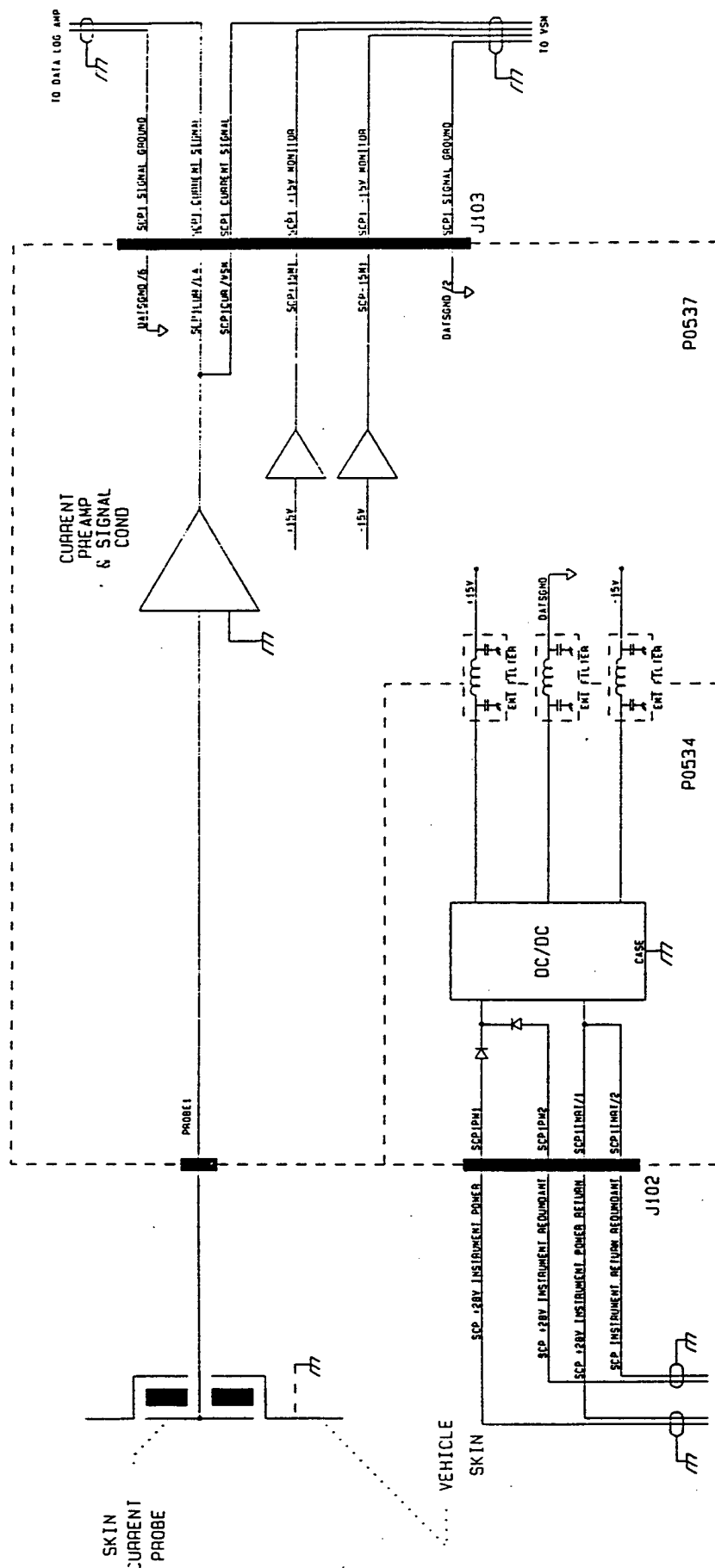
Figure 3-13. Electrical block diagram of skin current probe #1.

SKIN CURRENT PROBE - SC1

R8.63

4.50

2.90

3.38

8.00

6.50
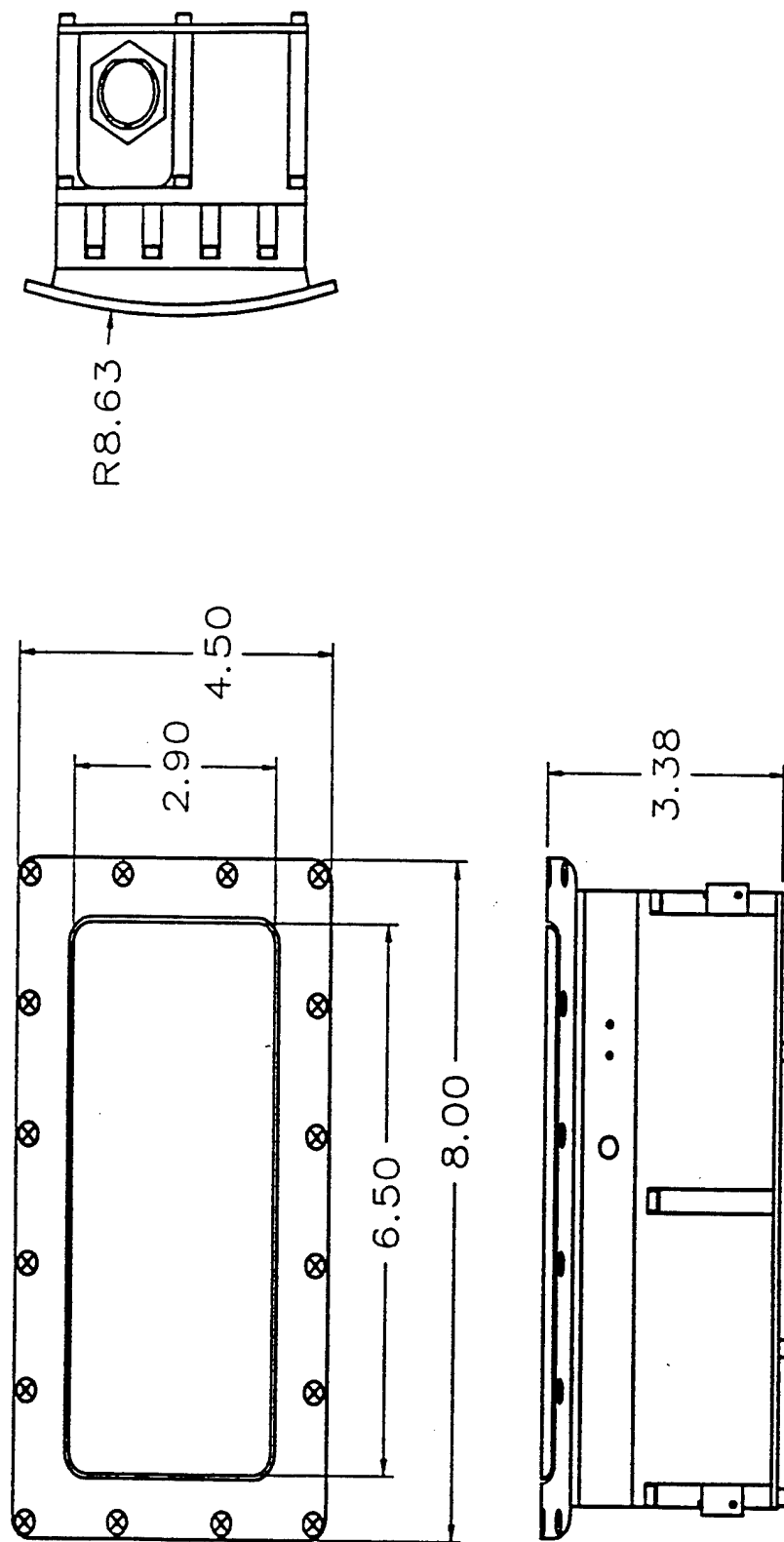
Figure 3-14.   Assembly drawing of skin current probe #1.

HIGH VOLTAGE BOOMS

FORWARD BAY SENSORS
    LLLTV – 1 (FORWARD CAMERA)
    OPTICAL SPECTROMETER

HIGH VOLTAGE MODULE

SCIENCE – 1 MODULE
    SKIN CURRENT PROBE
    DIFFERENTIAL CHARGING DEVICE
    CHARGED PARTICLE DETECTORS
    THERMIONIC EMITTER
    FIELD EMISSION DEVICE
    FAST DATA UNITS
    LLLTV – 2 (AFT CAMERA)
    SOLAR CELL EXPERIMENT

VEHICLE SERVICE MODULE

SCIENCE – 2 MODULE
    TRANSIENT PULSE MONITOR
    LANGMUIR PROBE
    FLOATING PROBE
    SKIN CURRENT PROBE
    GAS RELEASE SYSTEM
    PLASMA CONTACTOR SYSTEM
    NEUTRAL PRESSURE GAUGE

ATTITUDE CONTROL MODULE

ADAPTOR RING

Figure 3-15.   Instrument arrangement for SPEAR-3 payload.

31
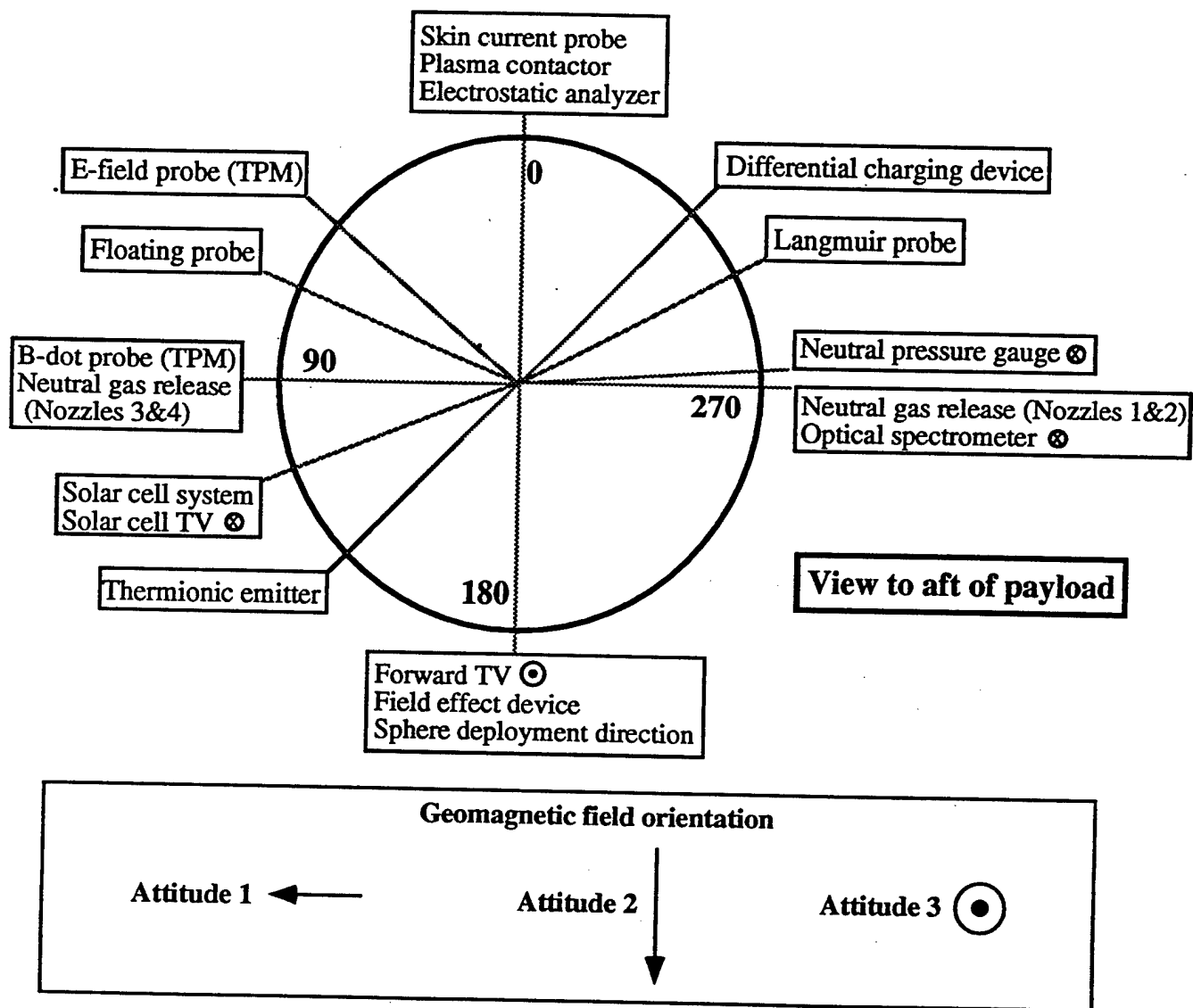
Figure 3-16. Azimuthal orientation of SPEAR-3 instruments with external access/viewing.

SPEAR-3
Electro-mechanical arrangement

Floating probe (16.4 mm diameter)

2.5 m
(Azimuthal direction 68° from direction shown)

0.44 m

Langmuir Probe
(Azimuthal direction 68° from direction shown)

Electrostatic Analyser
(15° x 5° FOV)

HV power supply

2 µF capacitor

5.2 m

Fiberglass boom

Graded boom

2.0 m

0.2 m
diameter

1.16 m
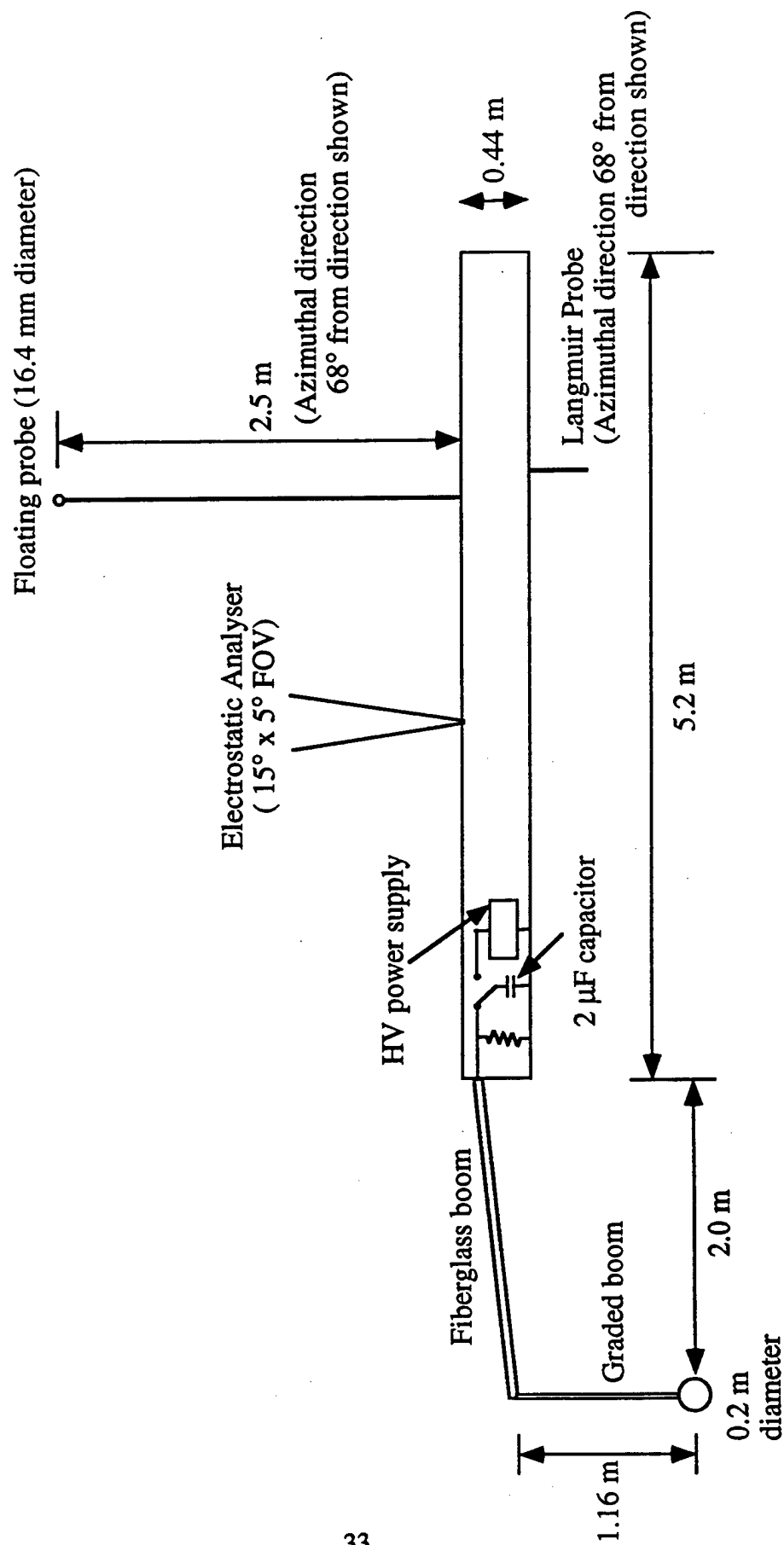
Figure 5-1. Electro-mechanical arrangement for SPEAR-3 biasing.
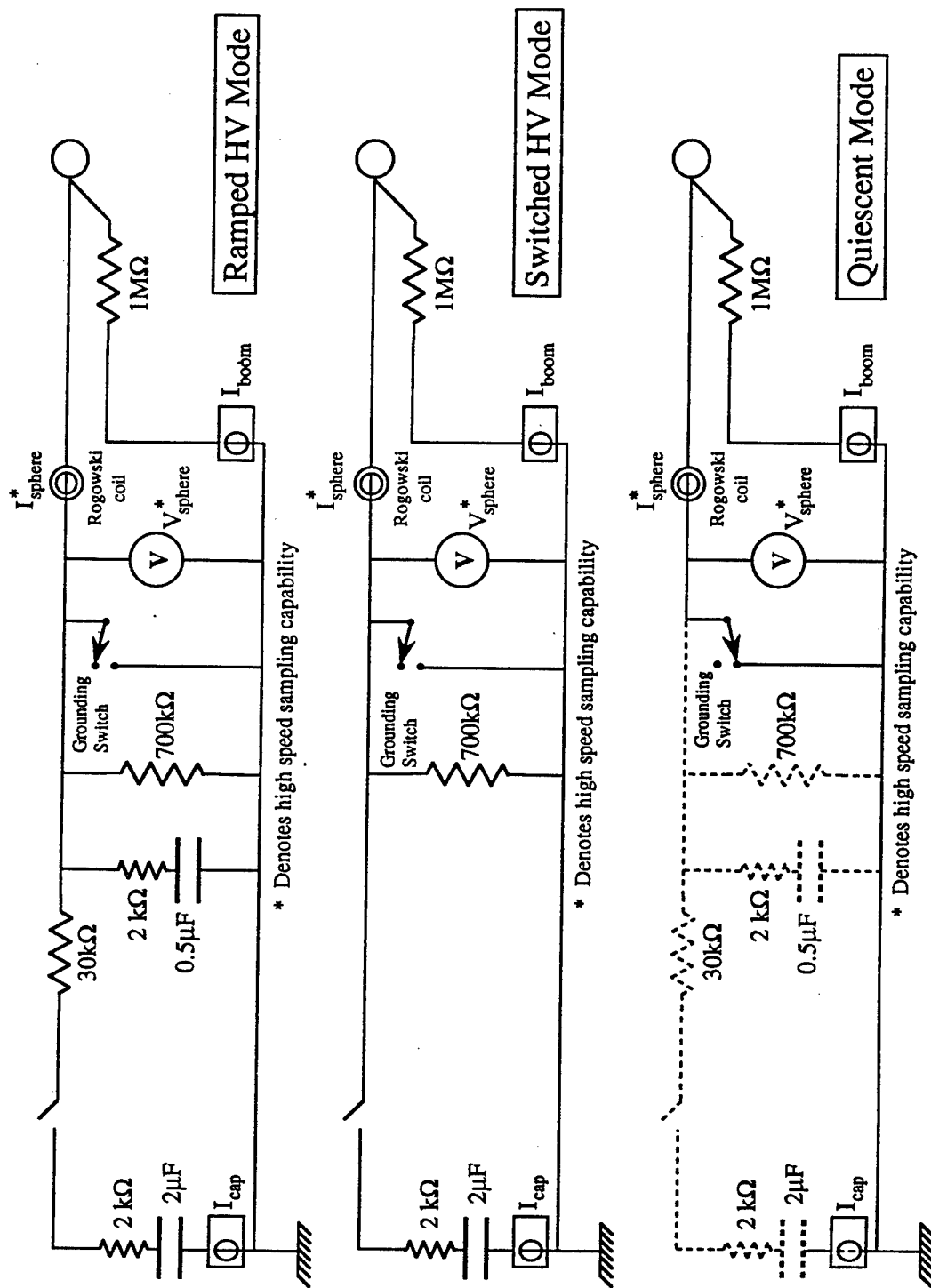
Ramped HV Mode

Switched HV Mode

Quiescent Mode

Figure 5-2. Simplified electrical schematic of ramped and switched HV modes.

SPEAR-3 Flight Trajectory and Attitudes
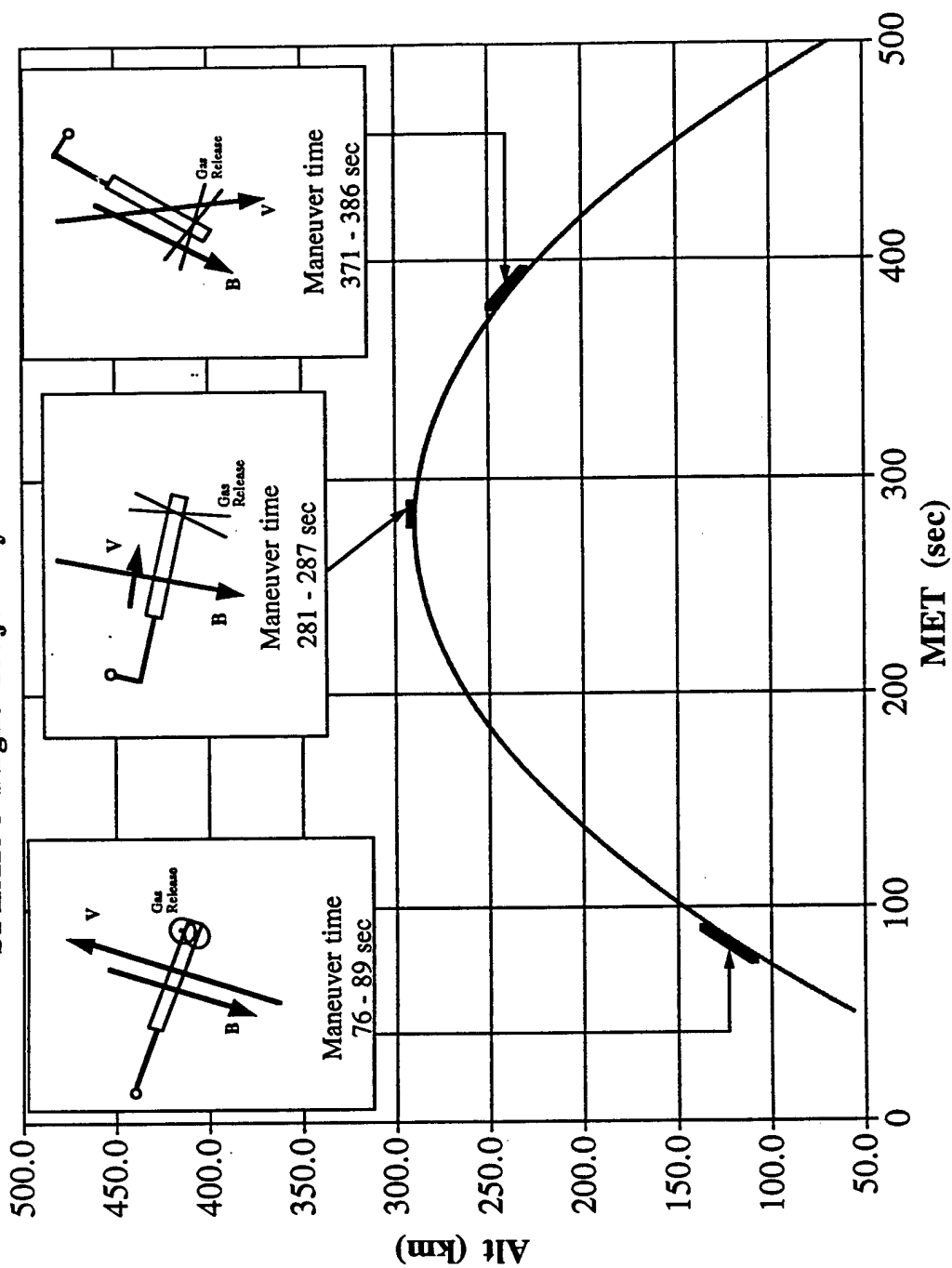
Figure 6-1. SPEAR-3 flight altitude trajectory and payload orientations.
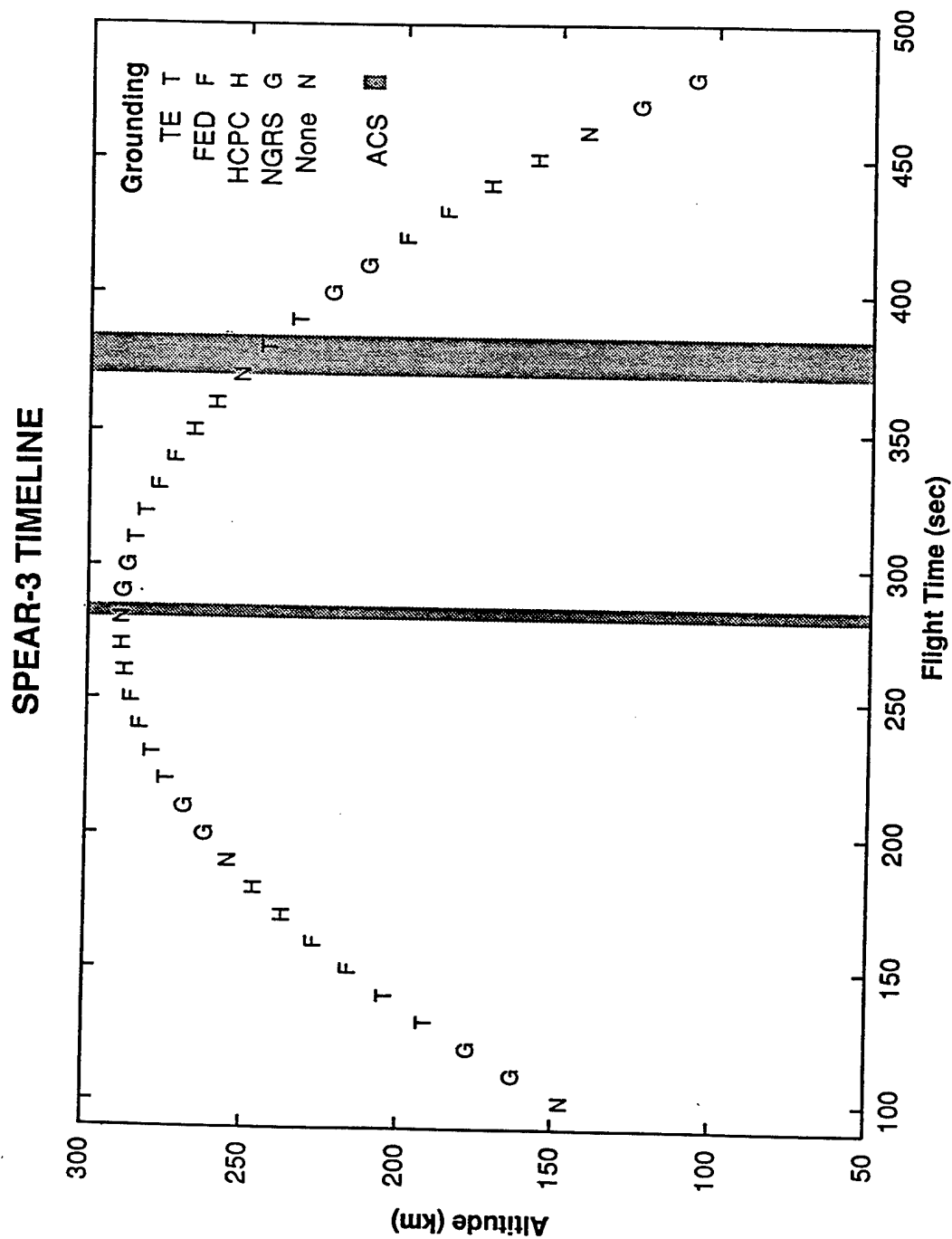
Figure 7-1. Timeline of grounding device operations.

Discharge
Relay

Grounding
Relay

Sphere

Sphere Sheath
Impedance

Ionospheric
Ground

2 kΩ

2μF

I_{cap}

700kΩ

I^*_{sphere}

Rogowski
coil

V^*_{sphere}

1MΩ (Graded boom)

Vehicle Sheath
Impedance

I_{boom}

Vehicle Ground

* Denotes high speed sampling capability
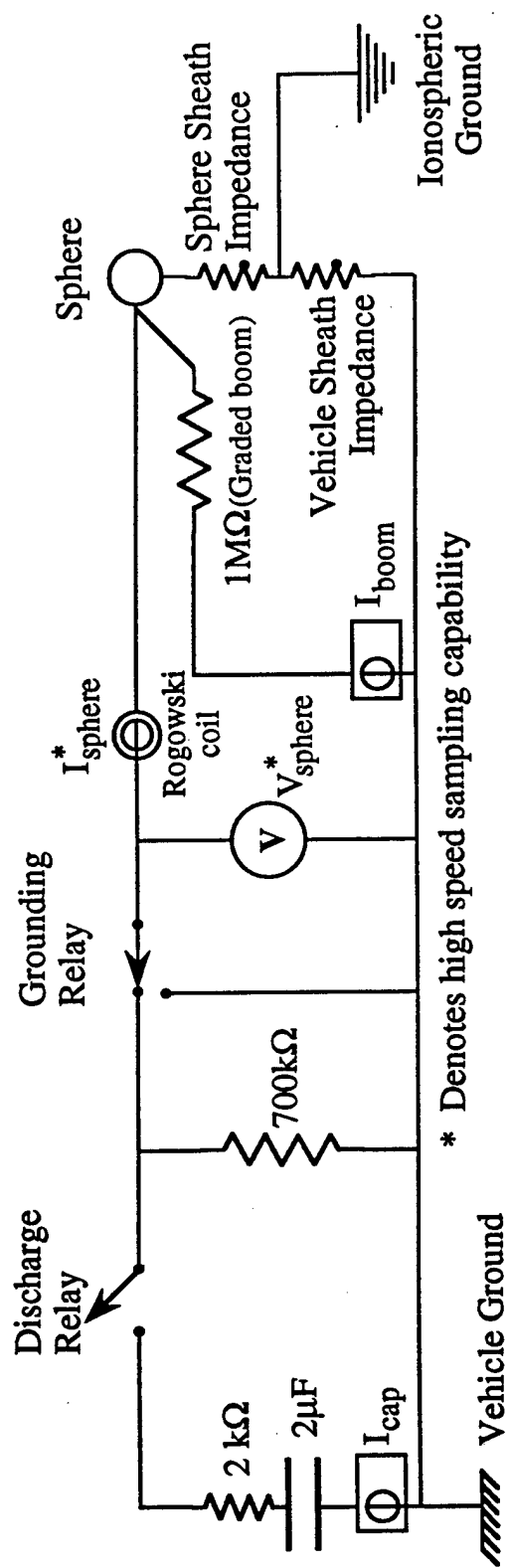
Simplified Schematic Diagram of HV System Showing Plasma Sheath Impedances

Figure 8-1. Simplified electrical schematic of HV system showing sheath impedances.

Figure 8-2. Variation of HV capacitor voltage for early (solid line) and later (broken line) periods in the flight.

SPEAR III NGRS GROUNDING
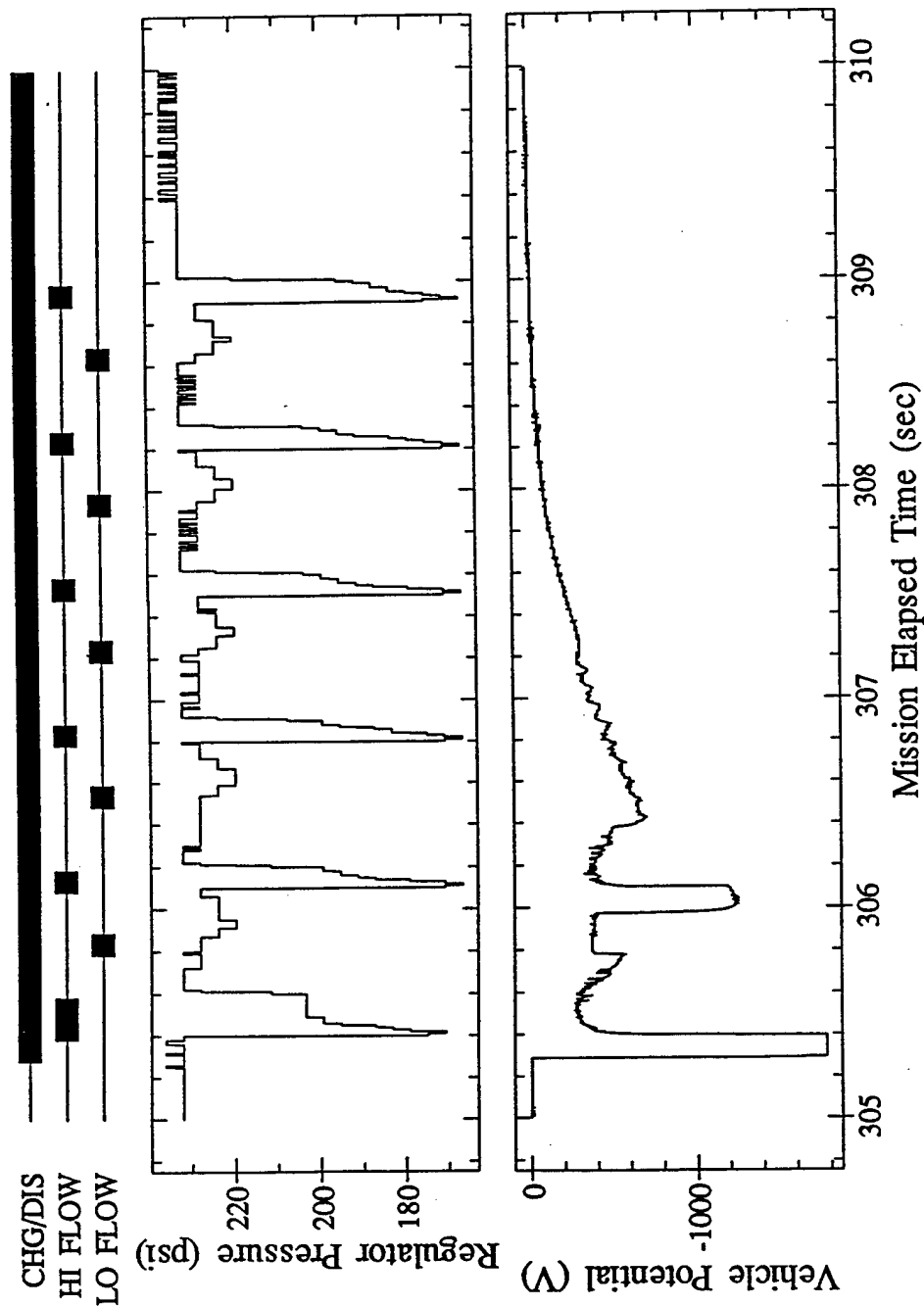
Figure 8-3. Variation of vehicle potential as a function of time when the neutral gas release system was active.

39
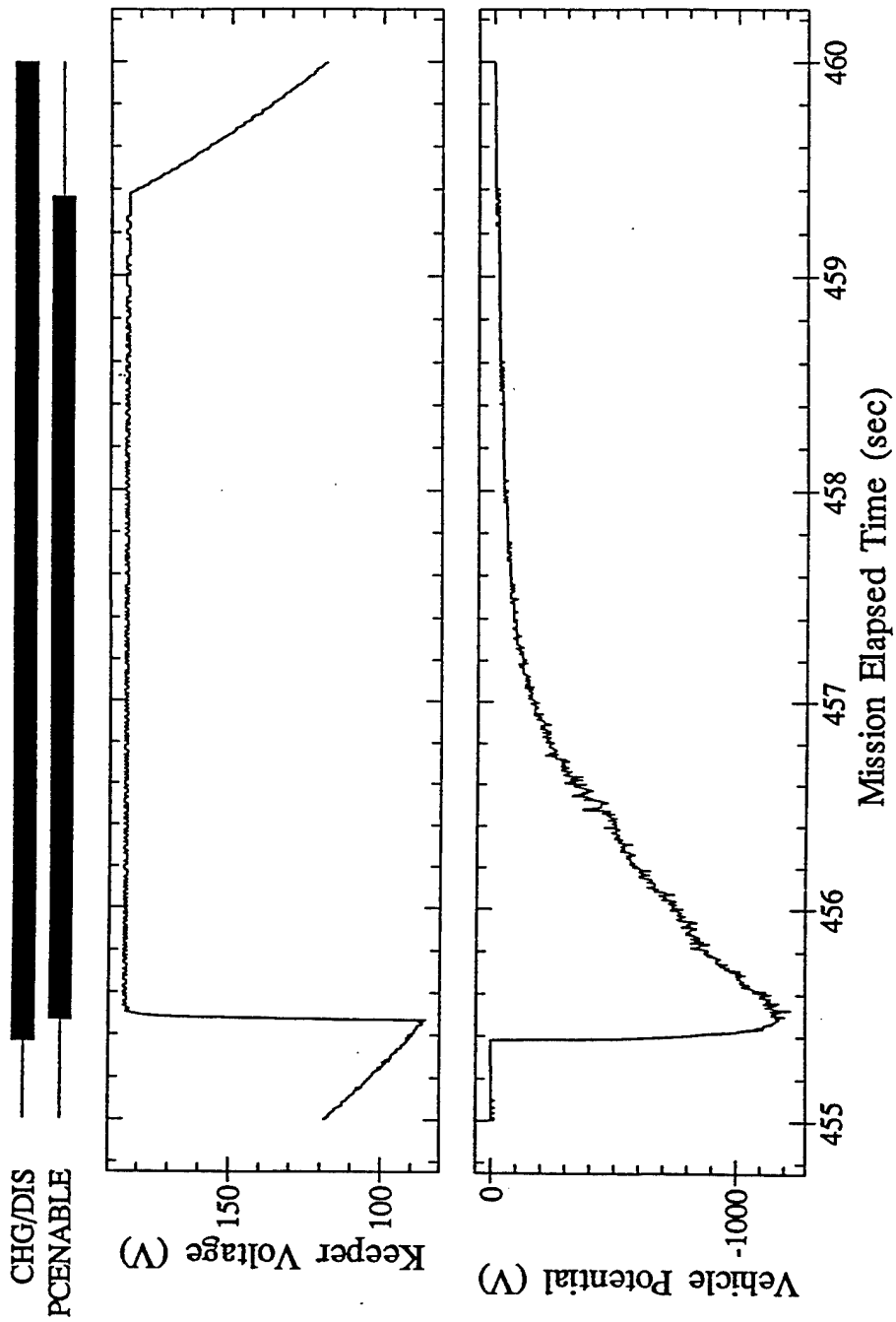
Figure 8-4. Variation of vehicle potential as a function of time when the hollow cathode plasma contactor was active.

40

SPEAR III TE GROUNDING
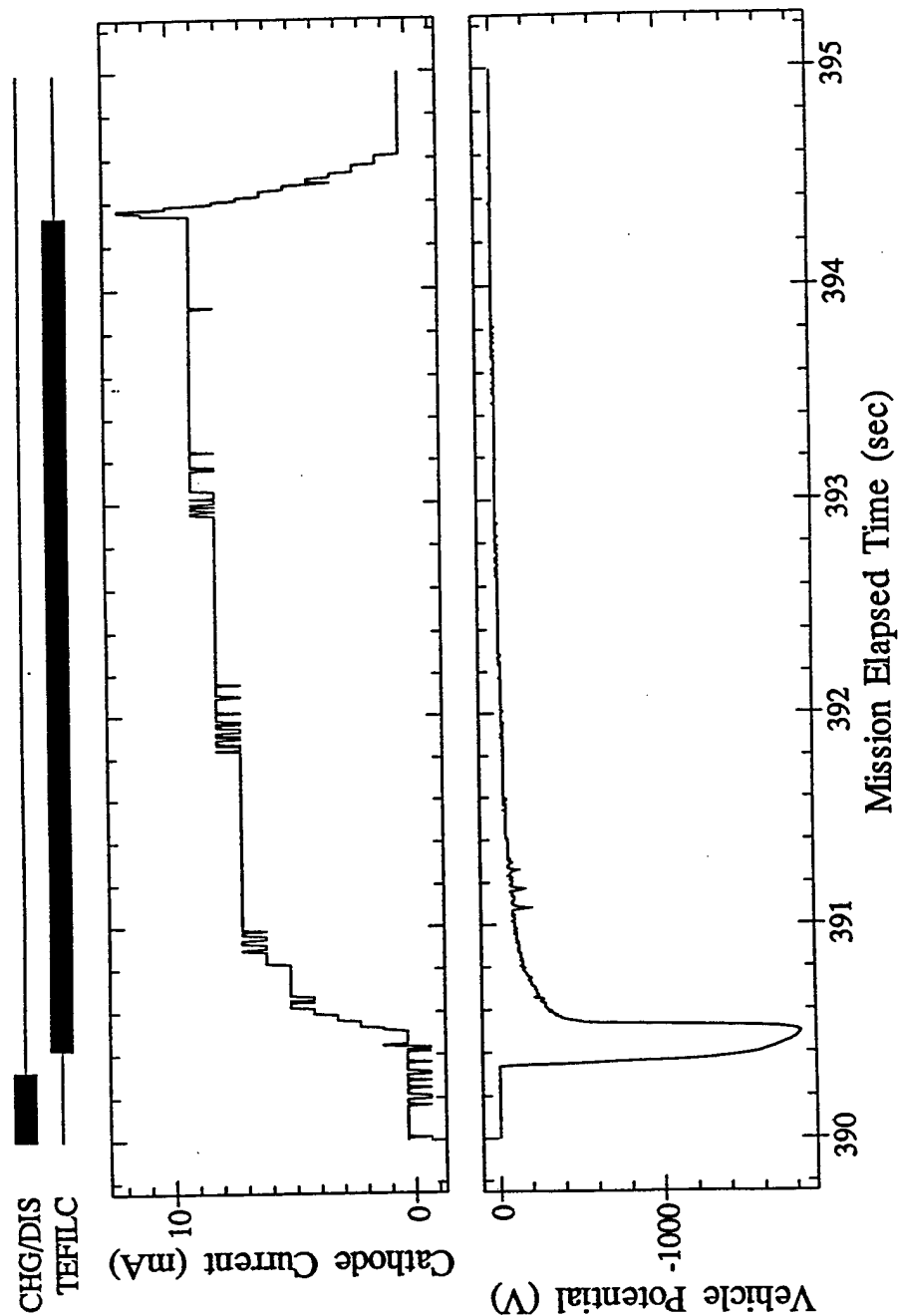
Figure 8-5. Variation of vehicle potential as a function of time when the thermionic emitter was active.

41
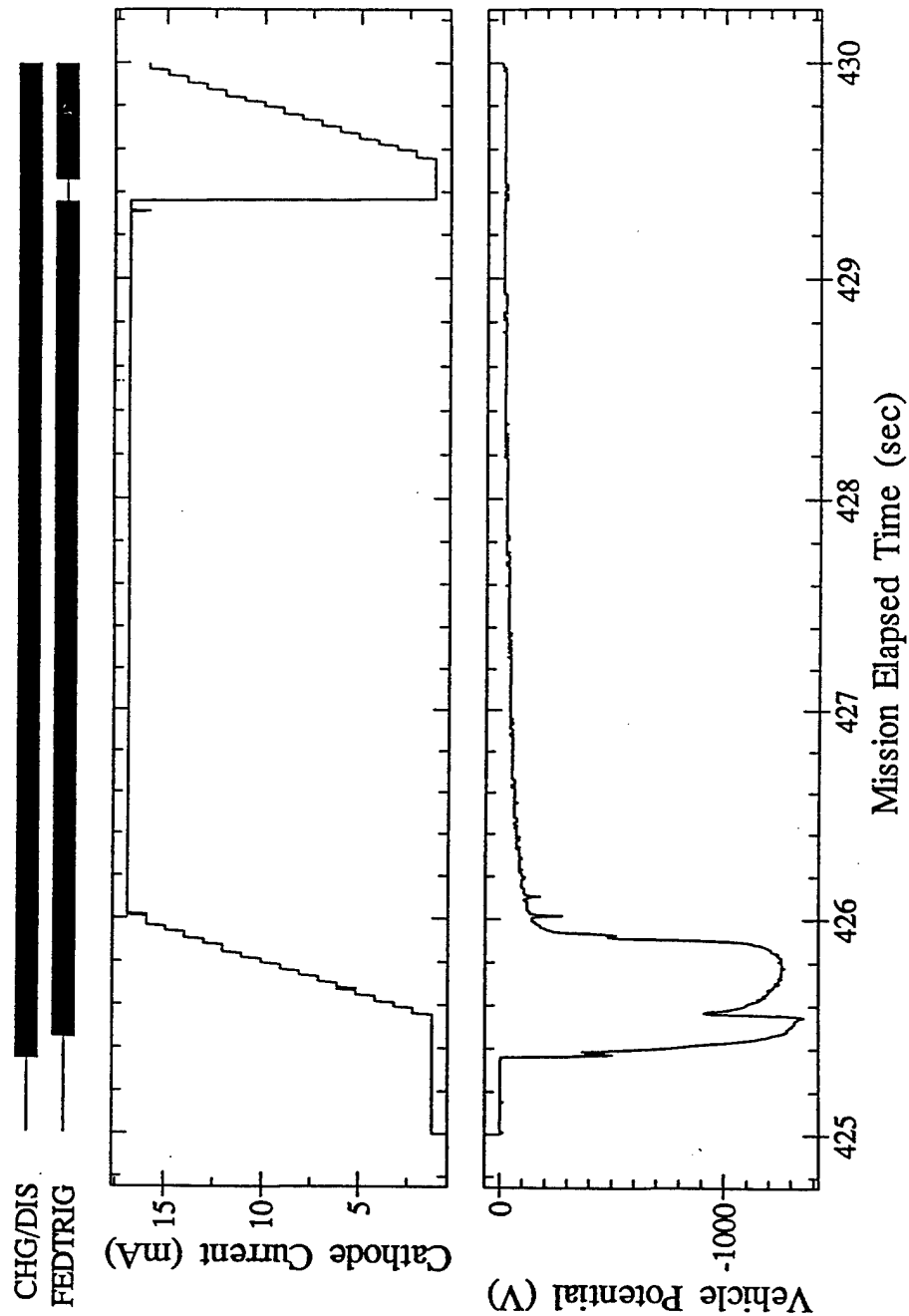
Figure 8-6. Variation of vehicle potential as a function of time when the field effect device was active.

42

SPEAR-3 Neutral Pressure Gauge
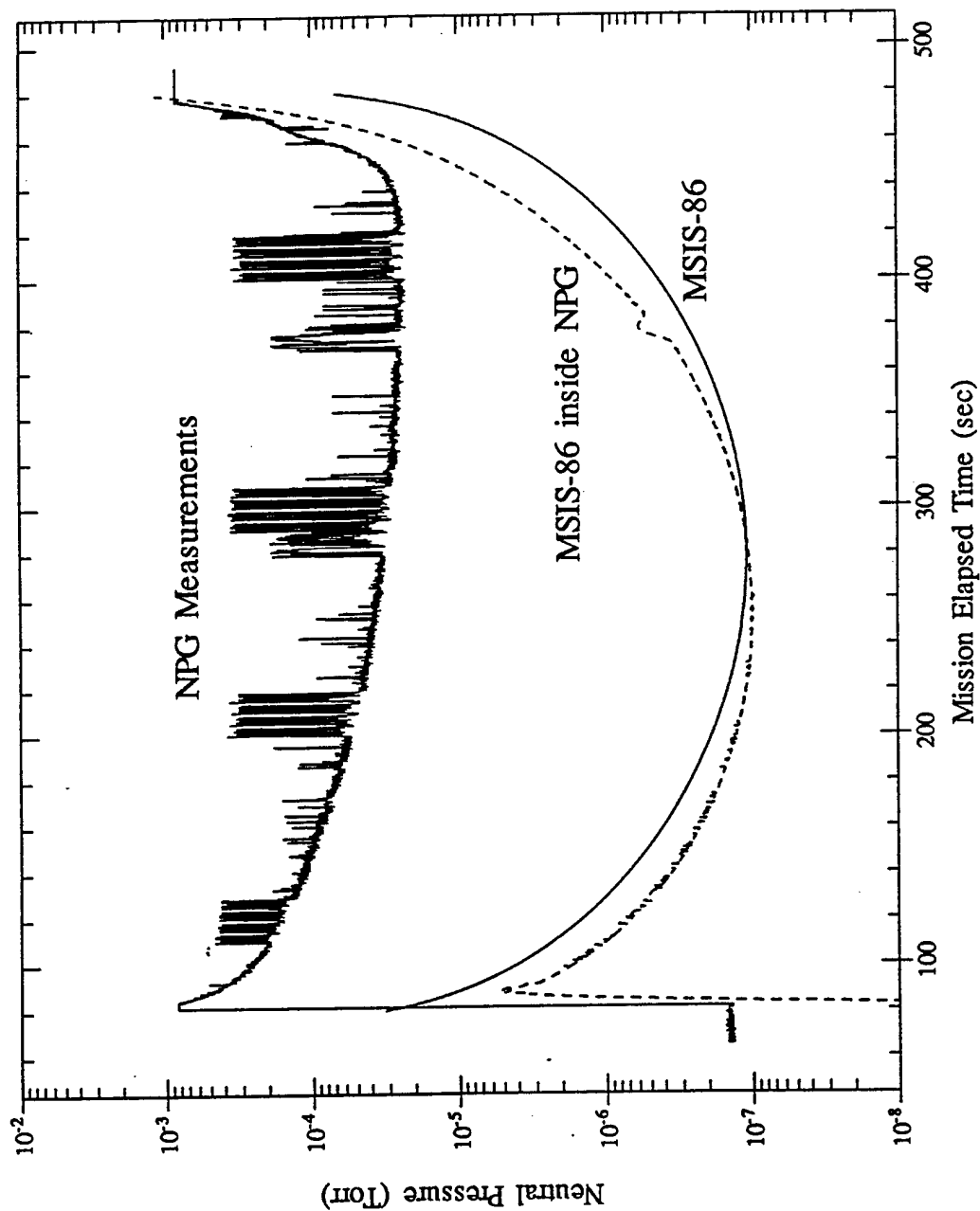
Figure 8-7. Comparison of neutral pressure gauge meausrements with the MSIS-86 model atmosphere outside the gauge and inside the gauge.

SPEAR-3
Electron Density v. Altitude
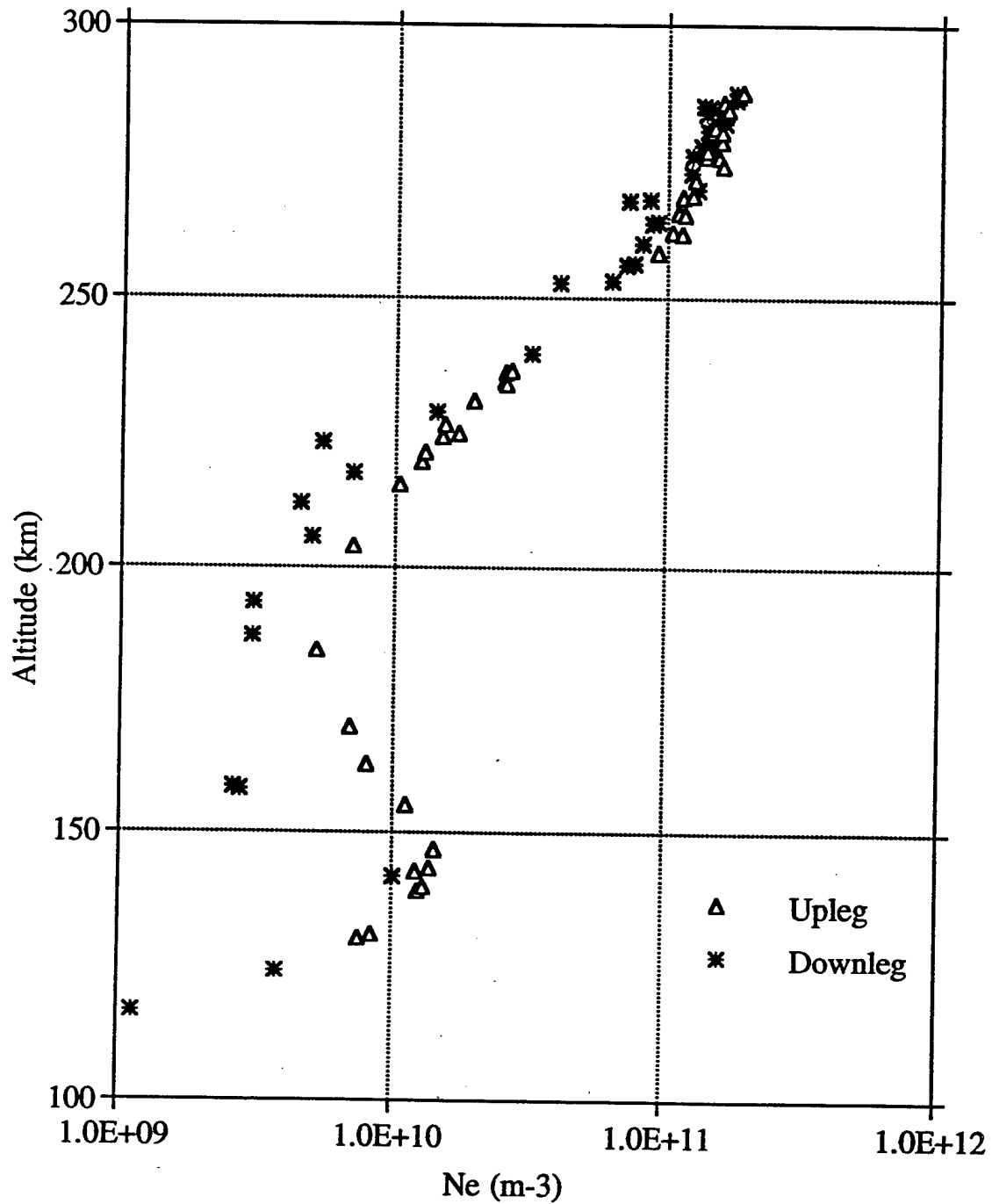
Figure 8-8. Electron density profiles deduced from Langmuir probe data.

SPEAR-3
Electron Temperature v. Altitude
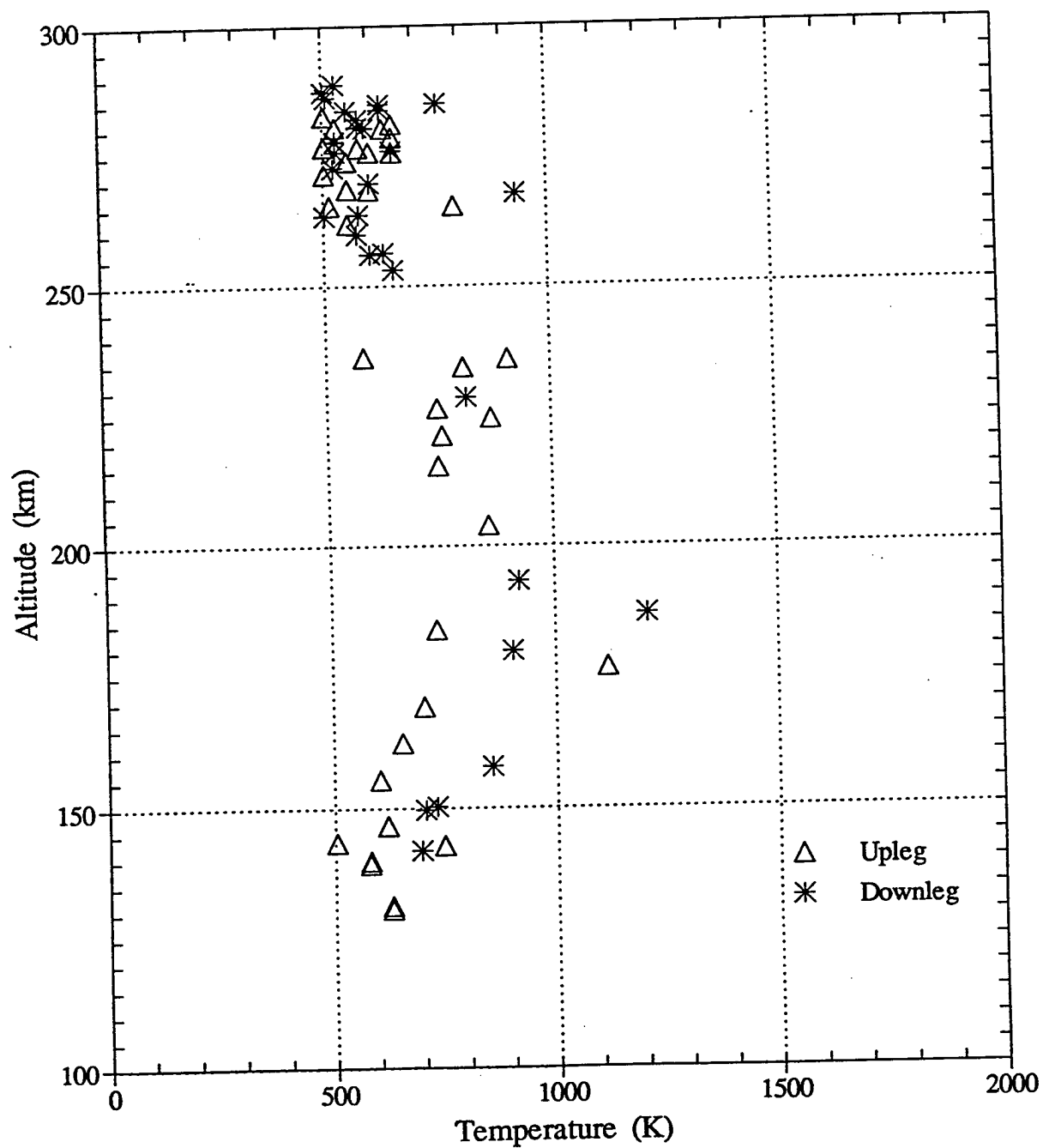
Figure 8-9. Electron temperatures deduced from Langmuir probe data.

APPENDIX A

LIST OF ABBREVIATIONS and ACRONYMS

angstrom	Å
attitude control system	ACS
charged coupled device	CCD
differential charge device	DCD
electron temperature	T_e
electrostatic analyzer	ESA
field effect device	FED
grams per second	g/sec
high voltage	HV
hollow cathode plasma contactor	HCPC
Kelvin	K
kilohertz	kHz
kilometers	km
kilohms	kΩ
kilovolt	kV
low-earth-orbit	LEO
low light level television	LLLTV
megahertz	MHz
megaohm	MΩ
meter	m
microamperes per square meter	$\mu A/m^2$
microfarads	μF
milliamp	mA
millimeters	mm
millisecond	msec
neutral gas release system	NGRS
neutral pressure gauge	NPG
pounds per square inch	psi
resistor capacitor	RC
skin current probe	SCP
space power experiments aboard rockets	SPEAR
thermionic emitter	TE

APPENDIX B

SPEAR-3 DATA ACCESS

The SPEAR-3 data archive at Utah State University.

The SPEAR-3 dataset is available on-line at Utah State University. It can be accessed via the internet. Telnet to "demise.cass.usu.edu" and log in with the username "spear" (if demise acts bogged down, you can also telnet to "malice.cass.usu.edu"). You will be prompted for the account password. Send e-mail to Don Thompson, "thompson@demise.cass.usu.edu", if you do not know the password. It will be changed periodically and e-mailed to those on the spear3 electronic mailing list. If you would like to be on this list, send a request to "thompson@demise.cass.usu.edu".

After logging in, you will be prompted for your terminal type. If your terminal type does vt100 emulation, just hit return. Otherwise enter your terminal type and hit return.

Next, you should change directories to your personal working directory, using the command "cd name", where 'name' is the name of your directory. If you do not have a personal directory, make one with the command "mkdir name" and then "cd name". When you are finished working on demise, issue "logout" to exit.

There are three data files available: "spear3_horiz.data", "spear3_vert.data", and "spear3_flight.data". The first two contain data taken during the horizontal and vertical tests at Phillips Lab. The third file contains the actual flight data.

These data files are binary. The files are formated similarly to the SPEAR-3 telemetry page, except that the time is appended to each minor frame. That is, the files are composed of fixed length records; 20 minor frames of 88 bytes. Bytes 1 through 77 are as defined in the telemetry page. Bytes 78, 79 and 80 are spares and reserved for future use. For the Phillips Lab data, bytes 80 and 81 are the SPEAR-3 sync word; for the flight data they are spares. Bytes 83 through 88 are the minor frame time, in BCD (binary coded decimal) as encoded by the tape digitizer (either Phillips lab or Wallops).

There is an extraction program available for use at Utah State University.

```
--------------------------------------------------
Using the USU/CASS PCM data reduction utility
--------------------------------------------------

Questions regarding the use of the data reduction utility
should be addressed via email to Don Thompson "thompson@usu.edu".

The following is a brief listing of usage:

spear3 {switches} {variables {variable_switches}}       ; for flight data
spear3_vert {switches} {variables {variable_switches}}  ; for vertical test
spear3_horiz {switches} {variables {variable_switches}} ; for horizontal test

variables:

Allowed variable names can be seen by issuing the command:
"more ~/spear3/spear3.setup".  Use the short name, the first column.

variable_switches:
```

-include lo hi	== Output only those values of the the variable that occur between lo and hi, must immediately follow the affected variable on the command line.
-exclude lo hi	== Output only those values of the the variable that occur outside lo and hi, must immediately follow the affected variable on the command line.

```
switches:
```

-input filename	== The name of a datafile to be used as input, defaults to the appropriate data file.
-from time	== The time to begin extraction, defaults to the beginning of the input file. Times are in seconds. If you are using gmt as the time then both from and to times can be entered in "ddd/hh:mm:ss.sss" format.
-to time	== The time to stop extraction, defaults to the end of input file.
-calibrate	== Forces simple calibrations to be applied to the telemetered data, this is the default.
-nocalibrate	== Extract raw, uncalibrated data.
-met	== Extract using MET as time, this is the default.
-gmt	== Extract using GMT as time.
-header	== Output data with simple header naming each column of numbers, this is the default.
-noheader	== No column name header output.

```
-oversample                    == Oversample low speed data.

-nooversample                  == Do not oversample low speed data,
                                  rather, subsample higher speed
                                  channels. This is the default.

-rate (rate)                   == The rate at which to sample the
                                  data, in Hertz.  Valid rates are;
                                  1, 2, 4, 5, 10, 20, 40, 50, 100,
                                  200, 400, 500, 1000, and 2000.
                                  Other values may work but will
                                  not result in evenly spaced sample
                                  intervals.

-binary                        == Produces binary output with met
                                  milliseconds as a big-endian
                                  four-byte integer followed by one
                                  byte for each of the specified
                                  channels.  This forces -nocalibrate,
                                  -met, -noplotl, and -noheader.

-nobinary                      == Produces ascii output.  This is
                                  the default.

-plot                          == Output plotl graphics commands
                                  instead of columns of numbers.
                                  The first variable on the command
                                  will be used as the x-axis,
                                  additional variables will be used
                                  as the y-axes in one or more panels.

-noplotl                       == Do not output graphics commands,
                                  this is the default.

-autoscale                     == Autoscale plots generated using
                                  plotl. This is only valid when
                                  the -plot switch has been used.
                                  This is the default

-fullscale                     == Use the channels full scale when
                                  plotting with the -plot switch,
                                  only valid in conjunction with
                                  the -plotl switch.

-symbols                       == Places a symbol at each data point
                                  when using plotl.  This is only
                                  valid when the -plot switch has
                                  been used.

-nosymbols                     == Does not place symbols on plotl
                                  plots.  This is the default.

-xgrid                         == Places gridlines at each x-axis tic
                                  mark when using plotl.  This is only
                                  valid when the -plot switch has been
                                  used.

-ygrid                         == Places gridlines at each y-axis tic
                                  mark when using plotl.  This is only
                                  valid when the -plot switch has been
                                  used.

-grid                          == Does both -xgrid and -ygrid.

-noxgrid                       == Does not print x-axis gridlines.
                                  This is the default.
```

```
        -noxgrid                        == Does not print y-axis gridlines.
                                           This is the default.

        -nogrid                         == Does both -noxgrid and -noygrid.
```

Examples:

```
spear3 -from 100 -to 105 logspher logscp1 > spear3.dat
```

Outputs time, log sphere voltage, and log skin current probe 1 current to the
file "spear3.dat" from 100 to 105 seconds.

```
spear3 -from 100 -to 105 met logspher logscp1 -plot1 | plot1 -s > spear3.ps
```

as above except that output is in the form of plot1 graphics commands
which are filtered by plot1, which generates PostScript code. The
code is saved in the file "spear3.ps" and is suitable for downloading
to any PostScript compatible printer. Note the inclusion of "met" on the
command line. This will plot logspher and logscp1 versus time. Excluding the
"met" would plot logscp1 versus logspher.

Note: plot1 is a plotting package available for use on demise.

Porting the USU/CASS extraction tool.

The extraction tool is written in FORTRAN. It should compile an run
on most unix computers, but it might not. The code is in spear3.f.
The files "spear3.include" and "spear3.defaults" are also required.

There are several possible problems.

First, the parameter nrecl in spear3.include may have to be changed,
depending on how the local computer treats the recordlength of random
acces files.

Second, the function millisec, which converts BCD to integer
milliseconds, is written assuming that integers are big-endian. That
is, Digital Equipment Corp., in its own way, swaps the bytes of
integer*2 numbers relative to how it's done on most computers. This
may need to be altered to be compatible with your computer.

Third, the startup line parameters are read with the routines
"iargc()" and "getarg()" which are provided as part of the f77 library
on DECstations and most Unix implementations of FORTRAN. They may not
be available on your local machine. If they are not you will need to
change all the startup line parameter reading code to more standard
FORTRAN read/write.

ShortName	Long Name	Cl	Rw	Int	Slope	Const.	Note
GMT	GMT	0	1	1	1	0	
MET	Mission Elapsed Time (sec)	0	1	1	1	0	
ALT	Altitude (km)	1	1	-1	CAL={-60.71112 2.55693 met		

mul add -4.88392e-03 met 2 exp mul add 1.03883e-06 met 3 exp mul add -9.27493e-10 m
et 4 exp mul add} TWOBYTES 1 1

| LAT | Latitude (deg) | 1 | 1 | -1 | CAL={37.86084 -8.73104e-04 | | |

met mul add -1.61157e-08 met 2 exp mul add -1.13083e-10 met 3 exp mul add -2.81644e
-13 met 4 exp mul add} TWOBYTES 1 1

| LON | East Longitude (deg) | 1 | 1 | -1 | CAL={-75.61688 5.35922e-03 | | |

met mul add -3.46924e-06 met 2 exp mul add 4.12015e-09 met 3 exp mul add -1.49243e-
13 met 4 exp mul add} TWOBYTES 1 1

ShortName	Long Name	Cl	Rw	Int	Slope	Const.	Note
ACSNZ	ASC Nozzle Discretes	11	1	1	1.0	0.0	
ACSNZ1 ERT	ACS 0 Deg Nozzle	11	1	1	1.0	0.0	BIT 0 INV
ACSNZ2 ERT	ACS 180 Deg Nozzle	11	1	1	1.0	0.0	BIT 1 INV
ACSNZ3 ERT	ACS 90 Deg Nozzle	11	1	1	1.0	0.0	BIT 2 INV
ACSNZ4 ERT	ACS 270 Deg Nozzle	11	1	1	1.0	0.0	BIT 3 INV
ACSNZ5 ERT	ACS CCWa Nozzle	11	1	1	1.0	0.0	BIT 4 INV
ACSNZ6 ERT	ACS CWa Nozzle	11	1	1	1.0	0.0	BIT 5 INV
ACSNZ7 ERT	ACS CWb Nozzle	11	1	1	1.0	0.0	BIT 6 INV
ACSNZ8 ERT	ACS CCWb Nozzle	11	1	1	1.0	0.0	BIT 7 INV
ACSPP	Pitch Position (Degrees)	12	1	20	1.412	-180.0	
ACSYP	Yaw Position (Degrees)	12	2	20	0.7059	-90.0	
ACSRP	Roll Position (Degrees)	12	3	20	1.412	-180.0	
ACSPR	Pitch Rate (Degrees/sec)	12	4	20	0.08824	-11.25	
ACSYR	Yaw Rate (Degrees/sec)	12	5	20	0.08824	-11.25	
ACSRR	Roll Rate (Degrees/sec)	12	6	20	0.08824	-11.25	
ACSPN	Pitch Error (Degrees)	12	7	20	0.04412	-5.625	
ACSYN	Yaw Error (Degrees)	12	8	20	0.04412	-5.625	
ACSRN	Roll Error (Degrees)	12	9	20	0.04412	-5.625	
ACSD	ACS Discretes (V)	36	10	20	0.01961	0.0	
ACSTPRES	Tank Pressure (psi)	36	11	20	19.61	0.0	
ACSIMP	Impulse (V)	36	13	20	0.01961	0.0	
ACSBM	ACS Battery Monitor (V)	36	14	20	0.03922	24.0	
SCSSER1	SCS Cell #1 Counter	24	1	20	1.0	0.0	TWOBYTES 24 2
SCSSER2	SCS Cell #2 Counter	24	6	20	1.0	0.0	TWOBYTES 24 7
SCSSER3	SCS Cell #3 Counter	24	11	20	1.0	0.0	TWOBYTES 24 12
SCSSER4	SCS Cell #4 Counter	24	16	20	1.0	0.0	TWOBYTES 24 17
SCSCUR1	SCS Cell #1 Current (uA)	32	2	2	0.07859	-11.03	
SCSCUR2	SCS Cell #2 Current (uA)	28	1	2	0.07929	-11.22	
SCSCUR3	SCS Cell #3 Current (uA)	28	2	2	0.07780	-10.88	
SCSCUR4	SCS Cell #4 Current (uA)	13	2	2	0.07722	-10.83	
SCS+15MB	SCS +15V B Monitor (V)	12	10	20	-0.3922	50.0	?
SCS-15MB	SCS -15V B Monitor (V)	12	11	20	-0.3922	50.0	
SCSHVMN	SCS 600V Monitor (V)	12	14	20	-7.843	1000.	
SCS+5MD	SCS +5V D Monitor (V)	12	17	20	0.03922	-5.0	?
SCSPRESS	SCS Pressure	50	17	20	-0.1421	16.30	
SCSDREJM	SCS Door Eject Monitor	59	3	20	1.0	0.0	BIT 0
ESADATA1	ESA Serial Data Out 1	18	1	1	1.0	0.0	
ESADATA2	ESA Serial Data Out 2	22	1	1	1.0	0.0	
ESADATA3	ESA Serial Data Out 3	26	1	1	1.0	0.0	
ESADATA4	ESA Serial Data Out 4	30	1	1	1.0	0.0	
ESADATA5	ESA Serial Data Out 5	34	1	1	1.0	0.0	
ESADATA6	ESA Serial Data Out 6	38	1	1	1.0	0.0	
ESADATA7	ESA Serial Data Out 7	42	1	1	1.0	0.0	

spear3.setup

Name	Description						
ESADATA8	ESA Serial Data Out 8	46	1	1	1.0	0.0	
ESASTEP	ESA Energy Step	18	1	1	CAL={ 0 esacal }		
ESACOUNTS1	ESA Channel 1 Counts	26	1	1	CAL={ 1 esacal }		
ESACOUNTS2	ESA Channel 2 Counts	30	1	1	CAL={ 2 esacal }		
ESACOUNTS3	ESA Channel 3 Counts	38	1	1	CAL={ 3 esacal }		
ESACOUNTS4	ESA Channel 4 Counts	42	1	1	CAL={ 4 esacal }		
ESAENERGY1	ESA Channel 1 Energy	18	1	1	CAL={ 5 esacal }		
ESAENERGY2	ESA Channel 2 Energy	18	1	1	CAL={ 6 esacal }		
ESAENERGY3	ESA Channel 3 Energy	18	1	1	CAL={ 7 esacal }		
ESAENERGY4	ESA Channel 4 Energy	18	1	1	CAL={ 8 esacal }		
ESAFLUX1	ESA Channel 1 FLUX	18	1	1	CAL={ 9 esacal }		
ESAFLUX2	ESA Channel 2 FLUX	18	1	1	CAL={10 esacal }		
ESAFLUX3	ESA Channel 3 FLUX	18	1	1	CAL={11 esacal }		
ESAFLUX4	ESA Channel 4 FLUX	18	1	1	CAL={12 esacal }		
#ESASTEP	ESA Energy Step	18	1	1	CAL={ v 127 iand dup 63 gt if 127 flip sub }		
#ESACOUNTS1	ESA Channel 1 Counts	26	1	1	CAL={ 34 row page 15 iand 256 mul v add }		
#ESACOUNTS2	ESA Channel 2 Counts	30	1	1	CAL={ 34 row page 240 iand 16 mul v add }		
#ESACOUNTS3	ESA Channel 3 Counts	38	1	1	CAL={ 46 row page 15 iand 256 mul v add }		
#ESACOUNTS4	ESA Channel 4 Counts	42	1	1	CAL={ 46 row page 240 iand 16 mul v add }		
ESAP15M	ESA +15V Monitor (V)	50	1	20	0.02020	12.03	
ESAM15M	ESA -15V Monitor (V)	50	2	20	0.01980	-18.09	
ESAP5M	ESA +5V Monitor (V)	50	3	20	0.01961	1.23	
ESABHVM	ESA HV Monitor (V)	50	4	20	-19.61	0.0	
ESAPSWHM	+High Sweep Monitor (V)	2	1	1	19.319	0.0	
ESAMSWHM	-High Sweep Monitor (V)	6	1	1	-19.679	0.0	
ESAPSWLM	+Low Sweep Monitor (V)	10	1	1	0.59843	0.0	
ESAMSWLM	-Low Sweep Monitor (V)	14	1	1	-0.61000	0.0	
ESASWPM	ESA Sweep Program Monitor (V)	50	5	20	0.1980	0.0	
ESATPWR	ESA LV Power Conv. Temp (DegC)	50	6	20	0.3765	-11.30	
ESATBHV	ESA Bias Pwr Conv. Temp (DegC)	50	7	20	0.3765	-11.30	
ESATSWP	ESA Sweep Conv Temp (DegC)	50	8	20	0.3765	-11.30	
ESATDIG	ESA Digital System Temp (DegC)	50	9	20	0.3765	-11.30	
ESATSAH	ESA Sensor 1 Temp (DegC)	50	10	20	0.3765	-11.30	
ESATSAL	ESA Sensor 2 Temp (DegC)	50	11	20	0.3765	-11.30	
ESATSBH	ESA Sensor 3 Temp (DegC)	50	12	20	0.3765	-11.30	
ESATSBL	ESA Sensor 4 Temp (DegC)	50	13	20	0.3765	-11.30	
ESATREG	ESA Sweep Regulator Temp (DegC)	50	14	20	0.3765	-11.30	
ESAD15M	ESA Delayed 15 Monitor	50	15	20	0.02039	12.34	
ESAD30M	ESA Delayed 30 Monitor	50	16	20	0.02039	26.40	
DCD+15MN	DCD +15V Monitor (V)	36	7	20	-0.3922	50.0	
DCD-15MN	DCD -15V Monitor (V)	36	8	20	-0.3922	50.0	
DCDHVMON	DCD High Voltage Monitor (V)	36	9	20	-0.3922	50.0	
DCDCUR	DCD Current (uA)	13	1	2	-0.7843	110.2	
DCDLIN/VSM	DCD Linear Voltage (V)	52	1	2	-19.61	2499.	
DCDLOG	DCD Log Voltage (V)	52	2	2	(c<108 ? -10.**(-0.03322*c +3.642) : c<148 ? 0.09373*c-11.47 : 10.**(0.03322*c-4.404)) FILE=/users/data4/spear/ spear3/DCDLOG.cal		
DCDPRESS	DCD Pressure	69	2	2	0.1421	-19.93	
DCDDREJM	DCD Door Eject Monitor	59	3	20	1.0	0.0	BIT 1
TEACTHIM	TE Cathode Current (mA)	29	1	2	0.9804	-22.22	
TEACBUSVM	TE AC Bus Voltage (Vrms)	12	18	20	0.1581	-3.839	
TEBIASVM	TE Bias Voltage (V)	12	19	20	0.1210	-2.741	
TEFILVM	TE Filament Voltage (V)	12	20	20	0.1544	-3.748	
TEFILIM	TE Filament Current (Arms)	36	1	20	0.06557	-1.582	
TEDREJM	TE Door Eject Monitor	59	3	20	1.0	0.0	BIT 2
FEDGATEI	FED Gate Current (uA)	31	1	2	15.81	-1816.	
FEDCATHI	FED Cathode Current (mA)	31	2	2	0.9804	-112.5	
FED+15MA	FED +15V A Monitor (V)	36	2	20	-0.3922	50.0	
FED-15MA	FED -15V A Monitor (V)	36	3	20	-0.3922	50.0	
FED+15MB	FED +15V B Monitor (V)	36	4	20	-0.3922	50.0	
FED-15MB	FED -15V B Monitor (V)	36	5	20	-0.3922	50.0	
FEDPRESS	FED Pressure	36	6	20	-0.1421	16.30	
FEDCATHV	FED Cathode Voltage (V)	32	1	2	-0.9839	112.8	

spear3.setup

FEDDREJM	FED Door Eject Monitor	59 3 20	1.0	0.0	BIT 3
GRTPM	NGRS Tank Pressure (psi)	72 15 20	12.217	-98.064	
GRTTM	NGRS Tank Temperature (DegC)	72 16 20	0.3247	-24.88	FILE=/use

rs/data4/spear/spear3/GRTTM.cal

GRREGPR	NGRS Regulator Pressure (psi)	59 9 20	4.0849	-41.667	
GRLOVM	NGRS Lo-Pressure Valve Mon	37 1 2	1.0	0.0	BIT 0
GRHIVM	NGRS Hi-Pressure Valve Mon	37 1 2	1.0	0.0	BIT 1
RNGIM	Ring (Boom) Current (mA)	39 1 2	0.4195	-7.002	
RNGVM	Ring (Boom) Voltage (V)	39 1 2	436.28	-7155.	
HVS1DM	Relay 1 Coil Voltage (V)	43 1 20	0.1673	-4.275	
HVS2DM	Relay 2 Coil Voltage (V)	43 2 20	0.1671	-4.269	
HVS3DM	Relay 3 Coil Voltage (V)	43 3 20	0.1674	-4.303	
HVS4DM	Relay 4 Coil Voltage (V)	43 4 20	0.1677	-4.276	
HVENDM	HV Enbl Relay Coil Voltage (V)	43 5 20	0.1664	-4.655	
LEDDM	LED Voltage (V)	43 6 20	0.1664	-4.662	
DISIM	Discharge Current (mA)	54 1 2	(c<153 ? 1.606*c-42.26 : 8		

.864*c-1151.) FILE=/users/data4/spear/spear3/DISIM.cal

CHGIM	Charge Current (mA)	43 8 20	0.08923	-2.389	
P28VM	+28V Monitor (V)	43 9 20	0.1847	-4.842	
P28IM	+28I Monitor (A)	43 10 20	0.07843	0.0	
P28VIM	Isolated +28V Monitor (V)	43 11 20	0.1850	-4.859	
P5VM	+5V Monitor (V)	43 12 20	0.02779	-0.7299	
P15VM	+15V Monitor (V)	43 13 20	0.08271	-2.172	
N15VM	-15V Monitor (V)	43 14 20	-0.08288	2.177	
PRES1M	Pressure 1 Monitor (psi)	43 15 20	0.07354	-1.875	
PRES2M	Pressure 2 Monitor (psi)	43 16 20	0.07354	-1.875	
HVPSVM	HV Power Supply Voltage (V)	43 17 20	47.58	-1211.	
HVPSIM	HV Power Supply Current (mA)	43 18 20	0.04726	-1.208	
ACVM	400 Hz AC Voltage (Vrms)	43 19 20	0.4669	6.429	
DCVM	+28V Int/Ext Monitor (V)	43 20 20	0.13495	0.0	
TV2ICCDM	LLLTV #2 ICCD AGC Monitor (V)	36 17 20	-0.01966	5.004	
TV2P12M	LLLTV #2 +12V Monitor (V)	36 18 20	(c<14 ? 0.5164*log((c+1.e-		

6)/6.543e-9) : 0.007025*c+10.99) FILE=/users/data4/spear/spear3/TV2P12M.cal

TV2PRESM	LLLTV #2 Pressure Monitor (psi)	36 19 20	0.06949	-1.634	
TV3ICCDM	LLLTV #3 ICCD AGC Monitor (V)	36 20 20	-0.01958	4.999	
TV3P12M	LLLTV #3 +12V Monitor (V)	59 1 20	(c<20 ? 0.4061*log((c+1.e-		

6)/2.605e-11) : 0.007131*c+10.96) FILE=/users/data4/spear/spear3/TV3P12M.cal

TV3PRESM	LLLTV #3 Pressure Monitor (psi)	59 2 20	0.06933	-1.674	
TV3SM	LLLTV #3 Shutter Mech.	37 1 2	1.0	0.0	BIT 2
TV3LVM	Illum. Lamp 12VDC Monitor (V)	59 4 20	(c<24 ? 0.3656*log((c+1.e-		

6)/1.562e-12) : 0.007106*c+10.93) FILE=/users/data4/spear/spear3/TV3LVM.cal

TV3LCM	Illum. Lamp Control Monitor	37 1 2	1.0	0.0	BIT 3
TV3DREJM	LLLTV #3 Door Eject Monitor	59 3 20	1.0	0.0	BIT 4
LPELEC	LP Electron Current (A)	15 1 1	(c<51 ? -2.982e-9*10**(-c/		

34.85) : 3.686e-12*10**(c/38.09)) FILE=/users/data4/spear/spear3/LPELEC.cal

LPION	LP Positive Ion Current (A)	21 1 1	0.02737	-9.5016	10**
LPSWEEP	LP Sweep Monitor (V)	20 1 1	0.01961	0.0	
LPVOLTS	LP Voltage (V)	20 1 1	0.02353	-1.0	
LPDEJM	LP Door Eject Monitor	59 3 20	1.0	0.0	BIT 5
LPDPLYM	LP Deploy Monitor	59 3 20	1.0	0.0	BIT 6
NPNPM	NPG Neutral Pressure (torr)	29 2 2	0.01494	-6.889	10**
NPTM	NPG Temperature (DegC)	23 2 2	0.3922	-40.0	
NPVPM	NPG Valve Position Monitor (%)	59 19 20	-1.4967	335.1	
NPDEJM	NPG Door Eject Monitor	59 3 20	1.0	0.0	BIT 7
NPDPLYM	NPG Deploy Monitor	59 7 20	1.0	0.0	BIT 0
TV1PRESM	OS Pressure Gauge (psi)	59 8 20	0.07206	-1.838	
TV1ICCDM	OS Gain (V)	37 2 2	0.03922	0.0	
PCPVMON	HCPC Power Supply Monitor	37 1 2	1.0	0.0	BIT 4
PCSYSI	HCPC System Current (mA)	59 11 20	1.683	0.0	
PCHEATV	HCPC Heater Voltage (V)	59 12 20	0.03020	0.0	
PCKEEPV	HCPC Keeper Voltage (V)	54 2 2	0.8549	0.0	
PCSYSTEMP	HCPC System Temperature	59 13 20	(40.82*(6.086-log(c)))		FIL

E=/users/data4/spear/spear3/PCSYSTEMP.cal

PCHEATI	HCPC Heater Current (A)	59 14 20	0.06953	0.0	
PCKEEPI	HCPC Keeper Current (mA)	55 1 2	7.003	0.0	
PCRETNI	HCPC Neutralize Current (mA)	3 1 -16	2.196	0.0	
PCINTPRES	HCPC Internal Pressure (torr)	55 2 2	0.6525	-46.95	
PCSUPPRES	HCPC Gas Supply Pressure (psi)	59 16 20	1.417	-59.99	

PCENCLPRES ̇ HCPC Enclosure Pressure (psi) 59 17 20 0.1043 0.0
PCDOOR HCPC Door Eject Monitor 59 7 20 1.0 0.0 BIT 1
PCDPLYM HCPC Deploy Monitor 59 7 20 1.0 0.0 BIT 2
SCP1+15M SCP #1 +15V Monitor (V) 72 17 20 -0.3922 50.0
SCP1-15M SCP #1 -15V Monitor (V) 72 18 20 -0.3922 50.0
SCP1CUR SCP #1 Current (mA) 23 1 2 -7.412e-3 0.9562
LOGSCP2 SCP #2 Log Current (mA) 27 1 2 (c<113 ? -10.**(-0.03224*c
+1.105) : c<147 ? 1.875e-4*c-0.02435 : 10.**(0.03224*c-7.193)) FILE=/users/data4/spe
ar/spear3/LOGSCP2.cal
SCP2+15M SCP #2 +15V Monitor (V) 72 19 20 -0.3922 50.0
SCP2-15M SCP #2 -15V Monitor (V) 72 20 20 -0.3922 50.0
SCP2CUR SCP #2 Current (mA) 27 2 2 (c<128 ? -0.08471*c+10.857
3 : -0.07647*c+9.8073) FILE=/users/data4/spear/spear3/SCP2CUR.cal
TPMPAMP1 Efield Pos. Amplitude (V/m) 60 1 2 1.0 0.0 10** FILE
=/users/data4/spear/spear3/TPMPAMP1.cal
TPMNAMP1 Efield Neg. Amplitude (V/m) 60 2 2 1.0 0.0 10** FILE
=/users/data4/spear/spear3/TPMNAMP1.cal
TPMPDER1 Efield Pos. Derivative (V/m-s) 61 1 2 1.0 0.0 10** FILE
=/users/data4/spear/spear3/TPMPDER1.cal
TPMNDER1 Efield Neg. Derivative (V/m-s) 61 2 2 1.0 0.0 10** FILE
=/users/data4/spear/spear3/TPMNDER1.cal
TPMINT1 Efield Integral (V-s/m) 62 1 2 1.0 0.0 10** FILE
=/users/data4/spear/spear3/TPMINT1.cal
TPMPAMP2 B-dot Pos. Amplitude (A/m) 62 2 2 1.0 0.0 10** FILE
=/users/data4/spear/spear3/TPMPAMP2.cal
TPMNAMP2 B-dot Neg. Amplitude (A/m) 63 1 2 1.0 0.0 10** FILE
=/users/data4/spear/spear3/TPMNAMP2.cal
TPMPDER2 B-dot Pos. Deriv. (A/m-s) 63 2 2 1.0 0.0 10** FILE
=/users/data4/spear/spear3/TPMPDER2.cal
TPMNDER2 B-dot Neg. Deriv. (A/m-s) 64 1 2 1.0 0.0 10** FILE
=/users/data4/spear/spear3/TPMNDER2.cal
TPMINT2 B-dot Integral (A-s/m) 64 2 2 1.0 0.0 10** FILE
=/users/data4/spear/spear3/TPMINT2.cal
TPMPAMP3 SCS Current Pos. Amplitude (A) 66 1 2 1.0 0.0 10** FILE
=/users/data4/spear/spear3/TPMPAMP3.cal
TPMNAMP3 SCS Current Neg. Amplitude (A) 66 2 2 1.0 0.0 10** FILE
=/users/data4/spear/spear3/TPMNAMP3.cal
TPMPDER3 SCS Current Pos. Deriv. (A/s) 68 1 2 1.0 0.0 10** FILE
=/users/data4/spear/spear3/TPMPDER3.cal
TPMNDER3 SCS Current Neg. Deriv. (A/s) 68 2 2 1.0 0.0 10** FILE
=/users/data4/spear/spear3/TPMNDER3.cal
TPMINT3 SCS Current Integral (A-s) 69 1 2 1.0 0.0 10** FILE
=/users/data4/spear/spear3/TPMINT3.cal
TPMHKP1 TPM Power Supply Temp. (deg C) 74 1 20 2.180 -295.8
TPMHKP2 TPM Processor Temp. (deg C) 74 2 20 2.180 -295.8
TPMHKP3 TPM Negative Supply Voltage (V) 74 3 20 0.1169 -14.9
TPMHKP4 TPM Positive Supply Voltage (V) 74 4 20 0.1153 -14.7
TPMHKP5 TPM E-Sensor Potential (V) 74 5 20 0.4588 -58.5
LOGSPHER Sphere Voltage (V) 40 1 2 1.0 0.0 FILE=/use
rs/data4/spear/spear3/LOGSPHER.cal
LOGROG Rogowski Current (mA) 40 2 2 1.0 0.0 FILE=/use
rs/data4/spear/spear3/LOGROG.cal
LOGSCP1 SCP #1 Log Current (mA) 70 1 2 (c<72 ? 10.**(-0.03922*c+0
..92) : c<186 ? -2.051e-4*c+0.02840 : -10.**(0.03922*c-9.30)) FILE=/users/data4/spear
/spear3/LOGSCP1.cal
DSPHSER HSDS Sphere Voltage (V) 4 1 -40 1.0 0.0 FILE=/use
rs/data4/spear/spear3/DSPHSER.cal
DROGSER HSDS Rogowski Current (mA) 7 1 -40 1.0 0.0 FILE=/use
rs/data4/spear/spear3/DROGSER.cal
DSCPSER HSDS SCP #1 Current (mA) 16 1 -40 1.0 0.0 FILE=/use
rs/data4/spear/spear3/LOGSCP1.cal
VSMMFS1 Minor Frame Sync #1 78 1 1 1.0 0.0
VSMMFS2 Minor Frame Sync #2 79 1 1 1.0 0.0
VSMMFS3 Minor Frame Sync #3 80 1 1 1.0 0.0
VSMSFID Sub Frame ID 58 1 1 1.0 0.0
VSMRFI VSM RF Power Inc 74 6 20 1.0 0.0
VSMRFR VSM RF Power Ref 74 7 20 1.0 0.0
VSM+5VM VSM +5V Monitor 74 8 20 1.0 0.0

spear3.setup

VSM+12VM	VSM +12V Monitor	74	9	20	1.0	0.0
VSM-12VM	VSM -12V Monitor	74	10	20	1.0	0.0
VSMTPB	VSM Temp PCM Box	74	11	20	1.0	0.0
VSMTEB	VSM Temp Electronics Box	74	12	20	1.0	0.0
VSMHSR	VSM Half Scale Ref	74	14	20	1.0	0.0
VSMHLP	VSM Hard Line Power	74	16	20	1.0	0.0
VSMDDCT	VSM DC/DC Conv Temp	74	17	20	1.0	0.0
VSMBV1	VSM Batt Voltage 1	74	18	20	1.0	0.0
VSMBV2	VSM Batt Voltage 2	74	19	20	1.0	0.0
VSMBV3	VSM Batt Voltage 3	74	20	20	1.0	0.0
VSMBV4	VSM Batt Voltage 4	77	1	20	1.0	0.0
VSMBV5	VSM Batt Voltage 5	77	2	20	1.0	0.0
VSMBV6	VSM Batt Voltage 6	77	3	20	1.0	0.0
VSMBV7	VSM Batt Voltage 7	77	4	20	1.0	0.0
VSMBV8	VSM Batt Voltage 8	77	5	20	1.0	0.0
VSMBV9	VSM Batt Voltage 9	77	6	20	1.0	0.0
VSMMPRES	VSM Motor Pressure	77	7	20	1.0	0.0
VSMMSCM1	VSM Squib Current #1	77	8	20	1.0	0.0
VSMMSCM2	VSM Squib Current #2	77	9	20	1.0	0.0
VSMXT1	VSM Link1 Xmtr Temp	77	16	20	1.0	0.0
VSMXT2	VSM Link2 Xmtr Temp	77	17	20	1.0	0.0
VSMXT3	VSM Link3 Xmtr Temp	77	18	20	1.0	0.0
VSMC5VM	VSM Controller 5V Monitor	77	19	20	1.0	0.0
VSMACC	VSM Accelerometer	77	20	20	1.0	0.0
VSMCC1	VSM Controller Clock 1	72	1	20	1.0	0.0
VSMCC2	VSM Controller Clock 2	72	2	20	1.0	0.0
VSMPT1	VSM Plate Temp 1	72	3	20	1.0	0.0
V44B	Bus 7 Int/Ext	72	5	20	1.0	0.0	BIT 1
V44C	Bus 6 Int/Ext	72	5	20	1.0	0.0	BIT 2
V44D	Bus 5 Int/Ext	72	5	20	1.0	0.0	BIT 3
V44E	Bus 4 Int/Ext	72	5	20	1.0	0.0	BIT 4
V44F	Bus 3 Int/Ext	72	5	20	1.0	0.0	BIT 5
V44G	Bus 2 Int/Ext	72	5	20	1.0	0.0	BIT 6
V44H	Bus 1 Int/Ext	72	5	20	1.0	0.0	BIT 7
V45A	OS Deploy Prim	72	6	20	1.0	0.0	BIT 0
V45B	HV Boom Release Sec	72	6	20	1.0	0.0	BIT 1
V45C	HV Boom Release Prim	72	6	20	1.0	0.0	BIT 2
V45D	Nose Cone Eject Sec	72	6	20	1.0	0.0	BIT 3
V45E	Nose Cone Eject Prim	72	6	20	1.0	0.0	BIT 4
V45F	Arm/Safe Sec	72	6	20	1.0	0.0	BIT 5
V45G	Arm/Safe Prim	72	6	20	1.0	0.0	BIT 6
V46A	TV3 Door Eject Prim	72	7	20	1.0	0.0	BIT 0
V46B	ESA Door Eject Sec	72	7	20	1.0	0.0	BIT 1
V46C	ESA Door Eject Prim	72	7	20	1.0	0.0	BIT 2
V46D	DCD/TE Door Eject Sec	72	7	20	1.0	0.0	BIT 3
V46E	DCD/TE Door Eject Prim	72	7	20	1.0	0.0	BIT 4
V46F	SCS Door Eject Sec	72	7	20	1.0	0.0	BIT 5
V46G	SCS Door Eject Prim	72	7	20	1.0	0.0	BIT 6
V46H	OS Deploy Sec	72	7	20	1.0	0.0	BIT 7
V47A	LP Door Eject Prim	72	8	20	1.0	0.0	BIT 0
V47B	FP Boom Deploy Sec	72	8	20	1.0	0.0	BIT 1
V47C	FP Boom Deploy Prim	72	8	20	1.0	0.0	BIT 2
V47D	FP Door Eject Sec	72	8	20	1.0	0.0	BIT 3
V47E	FP Door Eject Prim	72	8	20	1.0	0.0	BIT 4
V47F	FED Door Eject Sec	72	8	20	1.0	0.0	BIT 5
V47G	FED Door Eject Prim	72	8	20	1.0	0.0	BIT 6
V47H	TV3 Door Eject Sec	72	8	20	1.0	0.0	BIT 7
V48A	HV Control Arm/Safe Prim	72	9	20	1.0	0.0	BIT 0
V48B	NPG Door Eject Sec	72	9	20	1.0	0.0	BIT 1
V48C	NPG Door Eject Prim	72	9	20	1.0	0.0	BIT 2
V48D	HCPC Deploy Sec	72	9	20	1.0	0.0	BIT 3
V48E	HCPC Deploy Prim	72	9	20	1.0	0.0	BIT 4
V48F	HCPC Door Eject Sec	72	9	20	1.0	0.0	BIT 5
V48G	HCPC Door Eject Prim	72	9	20	1.0	0.0	BIT 6
V48H	LP Door Eject Sec	72	9	20	1.0	0.0	BIT 7
V49A	TE Filament	72	10	20	1.0	0.0	BIT 0
V49B	FED Simulator	72	10	20	1.0	0.0	BIT 1
V49C	FED Trigger	72	10	20	1.0	0.0	BIT 2

spear3.setup

V49D	TV2 LED	72 10 20	1.0	0.0	BIT 3
V49E	HV Enable	72 10 20	1.0	0.0	BIT 4
V49F	HV Connect/Disconnect	72 10 20	1.0	0.0	BIT 5
V49G	HV Network	72 10 20	1.0	0.0	BIT 6
V49H	HV Event Trigger	72 10 20	1.0	0.0	BIT 7
V50B	LLLTV3 Shutter	72 11 20	1.0	0.0	BIT 1
V50C	SCS HV Mode	72 11 20	1.0	0.0	BIT 2
V50D	SCS Test Mode	72 11 20	1.0	0.0	BIT 3
V50E	SCS Lamp	72 11 20	1.0	0.0	BIT 4
V50F	NGRS Hi Flow	72 11 20	1.0	0.0	BIT 5
V50G	NGRS Low Flow	72 11 20	1.0	0.0	BIT 6
V50H	DCD HV	72 11 20	1.0	0.0	BIT 7
V51B	NPG Motor Power	72 12 20	1.0	0.0	BIT 1
V51C	NPG Valve	72 12 20	1.0	0.0	BIT 2
V51D	NPG HV	72 12 20	1.0	0.0	BIT 3
V51E	HCPC Gas Valve	72 12 20	1.0	0.0	BIT 4
V51F	HCPC Enable/Disable	72 12 20	1.0	0.0	BIT 5
V51G	HCPC Preheater	72 12 20	1.0	0.0	BIT 6
V51H	HCPC Heater	72 12 20	1.0	0.0	BIT 7
V52A	ESA Inst Power	72 13 20	1.0	0.0	BIT 0
V52B	SCP Inst Power	72 13 20	1.0	0.0	BIT 1
V52C	TE Inst Power	72 13 20	1.0	0.0	BIT 2
V52D	HSDS Inst Power	72 13 20	1.0	0.0	BIT 3
V52E	OS Inst Power	72 13 20	1.0	0.0	BIT 4
V52F	TV3 Inst Power	72 13 20	1.0	0.0	BIT 5
V52G	TV2 Inst Power	72 13 20	1.0	0.0	BIT 6
V52H	HV Inst Power	72 13 20	1.0	0.0	BIT 7
V53A	LP Inst Power	72 14 20	1.0	0.0	BIT 0
V53B	DCD Service Power	72 14 20	1.0	0.0	BIT 1
V53C	DCD Inst Power	72 14 20	1.0	0.0	BIT 2
V53D	FED Service Power	72 14 20	1.0	0.0	BIT 3
V53E	FED Inst Power	72 14 20	1.0	0.0	BIT 4
V53F	SCS Service Power	72 14 20	1.0	0.0	BIT 5
V53G	SCS Inst Power	72 14 20	1.0	0.0	BIT 6
V53H	ESA Delayed Power	72 14 20	1.0	0.0	BIT 7
V54A	Xmit #1 Power	77 10 20	1.0	0.0	BIT 0
V54B	VSM Inst Power	77 10 20	1.0	0.0	BIT 1
V54C	NGRS Inst Power	77 10 20	1.0	0.0	BIT 2
V54D	HCPC Service Power	77 10 20	1.0	0.0	BIT 3
V54E	HCPC Inst Power	77 10 20	1.0	0.0	BIT 4
V54F	FP Inst Power	77 10 20	1.0	0.0	BIT 5
V54G	TPM Inst Power	77 10 20	1.0	0.0	BIT 6
V54H	NPG Inst Power	77 10 20	1.0	0.0	BIT 7
V55A	SCS Test Mode	77 11 20	1.0	0.0	BIT 0
V55B	SCP Cal Mode	77 11 20	1.0	0.0	BIT 1
V55C	Event Trigger	77 11 20	1.0	0.0	BIT 2
V55D	Event Trigger	77 11 20	1.0	0.0	BIT 3
V55E	Event Trigger	77 11 20	1.0	0.0	BIT 4
V55F	Radar Beacon Power	77 11 20	1.0	0.0	BIT 5
V55G	Xmit #3 Power	77 11 20	1.0	0.0	BIT 6
V55H	Xmit #2 Power	77 11 20	1.0	0.0	BIT 7
V56A	HV Control Arm/Safe Sec	77 12 20	1.0	0.0	BIT 0
V56A	HV Control Arm/Safe Sec	77 12 20	1.0	0.0	BIT 0
OSDPLYP	OS Deploy Prim	72 6 20	1.0	0.0	BIT 0
HVBRS	HV Boom Release Sec	72 6 20	1.0	0.0	BIT 1
HVBRP	HV Boom Release Prim	72 6 20	1.0	0.0	BIT 2
NTES	Nose Cone Eject Sec	72 6 20	1.0	0.0	BIT 3
NTEP	Nose Cone Eject Prim	72 6 20	1.0	0.0	BIT 4
PARMS	Arm/Safe Sec	72 6 20	1.0	0.0	BIT 5
PARMP	Arm/Safe Prim	72 6 20	1.0	0.0	BIT 6
TV3DEJP	TV3 Door Eject Prim	72 7 20	1.0	0.0	BIT 0
ESADEJS	ESA Door Eject Sec	72 7 20	1.0	0.0	BIT 1
ESADEJP	ESA Door Eject Prim	72 7 20	1.0	0.0	BIT 2
DCDTEDEJS	DCD/TE Door Eject Sec	72 7 20	1.0	0.0	BIT 3
DCDTEDEJP	DCD/TE Door Eject Prim	72 7 20	1.0	0.0	BIT 4
SCSDEJS	SCS Door Eject Sec	72 7 20	1.0	0.0	BIT 5
SCSDEJP	SCS Door Eject Prim	72 7 20	1.0	0.0	BIT 6
OSDPLYS	OS Deploy Sec	72 7 20	1.0	0.0	BIT 7

spear3.setup

LPDEJP	LP Door Eject Prim	72	8	20	1.0	0.0	BIT 0
FPDPLYS	FP Boom Deploy Sec	72	8	20	1.0	0.0	BIT 1
FPDPLYP	FP Boom Deploy Prim	72	8	20	1.0	0.0	BIT 2
FPDEJS	FP Door Eject Sec	72	8	20	1.0	0.0	BIT 3
FPDEJP	FP Door Eject Prim	72	8	20	1.0	0.0	BIT 4
FEDDEJS	FED Door Eject Sec	72	8	20	1.0	0.0	BIT 5
FEDDEJP	FED Door Eject Prim	72	8	20	1.0	0.0	BIT 6
TVEDEJS	TV3 Door Eject Sec	72	8	20	1.0	0.0	BIT 7
HVARMP	HV Control Arm/Safe Prim	72	9	20	1.0	0.0	BIT 0
NPGDEJS	NPG Door Eject Sec	72	9	20	1.0	0.0	BIT 1
NPGDEJP	NPG Door Eject Prim	72	9	20	1.0	0.0	BIT 2
PCDPLYS	HCPC Deploy Sec	72	9	20	1.0	0.0	BIT 3
PCDPLYP	HCPC Deploy Prim	72	9	20	1.0	0.0	BIT 4
PCDEJS	HCPC Door Eject Sec	72	9	20	1.0	0.0	BIT 5
PCDEJP	HCPC Door Eject Prim	72	9	20	1.0	0.0	BIT 6
LPDEJS	LP Door Eject Sec	72	9	20	1.0	0.0	BIT 7
TEFILC	TE Filament	72	10	20	1.0	0.0	BIT 0
FEDSIM	FED Simulator	72	10	20	1.0	0.0	BIT 1
FEDTRIG	FED Trigger	72	10	20	1.0	0.0	BIT 2
ILULED	TV2 LED	72	10	20	1.0	0.0	BIT 3
HVENABL	HV Enable	72	10	20	1.0	0.0	BIT 4
SPHCON	HV Connect/Disconnect	72	10	20	1.0	0.0	BIT 5
DCHGNET	HV Network	72	10	20	1.0	0.0	BIT 6
CHGDIS	HV Event Trigger	72	10	20	1.0	0.0	BIT 7
TV3SC	LLLTV3 Shutter	72	11	20	1.0	0.0	BIT 1
SCS600RL	SCS HV Mode	72	11	20	1.0	0.0	BIT 2
SCSRELAY	SCS Test Mode	72	11	20	1.0	0.0	BIT 3
TV3LC	SCS Lamp	72	11	20	1.0	0.0	BIT 4
GRHPVC	NGRS Hi Flow	72	11	20	1.0	0.0	BIT 5
GRLPVC	NGRS Low Flow	72	11	20	1.0	0.0	BIT 6
DCDHVREL	DCD HV	72	11	20	1.0	0.0	BIT 7
NPVPWR	NPG Motor Power	72	12	20	1.0	0.0	BIT 1
NPVC	NPG Valve	72	12	20	1.0	0.0	BIT 2
NPHVCNTRL	NPG HV	72	12	20	1.0	0.0	BIT 3
PCGASONOFF	HCPC Gas Valve	72	12	20	1.0	0.0	BIT 4
PCENABLE	HCPC Enable/Disable	72	12	20	1.0	0.0	BIT 5
PCPHTR	HCPC Preheater	72	12	20	1.0	0.0	BIT 6
PCHTRON	HCPC Heater	72	12	20	1.0	0.0	BIT 7
XMIT1P	Xmit #1 Power	77	10	20	1.0	0.0	BIT 0
XMIT2P	Xmit #2 Power	77	11	20	1.0	0.0	BIT 7
XMIT3P	Xmit #3 Power	77	11	20	1.0	0.0	BIT 6
ESAVSMFS	ESA Full-Scale Reference	50	19	20	1.0	0.0	
ESAVSMHS	ESA Half-Scale Reference	50	20	20	1.0	0.0	
FPHF21	FP High Frequency V21 (V)	1	1	-8	0.7608	-97.0	
FPV12M	FP V12 Medium Gain (V)	8	1	-40	-1.5196	194.0	
FPV21H	FP V21 High Gain (V)	70	2	2	0.1900	-24.2	
FPV21L	FP V21 Low Gain (V)	71	1	2	12.157	-1550.0	
FPV12L	FP V12 Low Gain (V)	71	1	2	-12.157	1550.0	
FPV1S	FP V1S Medium Gain (V)	71	2	2	-3.2353	115.0	
FPDEJM	FP Door Eject Monitor	59	7	20	1.0	0.0	BIT 3
FPDPLYMC	FP Limit Switch Common	59	7	20	1.0	0.0	BIT 4
BYTE3	TM Page byte 3	3	1	1	1.0	0.0	
BYTE19	TM Page byte 19	19	1	1	1.0	0.0	
BYTE35	TM Page byte 35	35	1	1	1.0	0.0	
BYTE51	TM Page byte 51	51	1	1	1.0	0.0	
BYTE67	TM Page byte 67	67	1	1	1.0	0.0	
BYTE83	TM Page byte 83	83	1	1	1.0	0.0	
BYTE84	TM Page byte 84	84	1	1	1.0	0.0	
BYTE85	TM Page byte 85	85	1	1	1.0	0.0	
BYTE86	TM Page byte 86	86	1	1	1.0	0.0	
BYTE87	TM Page byte 87	87	1	1	1.0	0.0	
BYTE88	TM Page byte 88	88	1	1	1.0	0.0	

```
FPV21L_FIX     FP V21 Low Gain Fixed (V)     71  1   2    CAL={ -1550 12.157 v mul a
dd 79 2 rowoffset 20 div int 20 mul add page 256 mul 80 2 rowoffset 20 div int 20 mu
l add page add 10000 sub sub }
FPV12L_FIX     FP V12 Low Gain Fixed (V)     71  1   2    CAL={ -1550 12.157 v mul a
dd 79 2 rowoffset 20 div int 20 mul add page 256 mul 80 2 rowoffset 20 div int 20 mu
l add page add 10000 sub sub -1 mul}
```

spear3.setup

```
ESA_PEAK        ESA Derived Vehicle Potential    79  3  20   0.2 0.0 TWOBYTES 80 3
ESA_FLUX        ESA Integrated Ion Flux          79 14  20   CAL={ v 10 80 14 mpage 1 s
ub exp mul }
MSIS_HE         MSIS He Density (m^-3)           79  4  20   0.001 0.0 10** TWOBYTES 80
 4
MSIS_O          MSIS O Density (m^-3)            79  5  20   0.001 0.0 10** TWOBYTES 80
 5
MSIS_N2         MSIS N2 Density (m^-3)           79  6  20   0.001 0.0 10** TWOBYTES 80
 6
MSIS_O2         MSIS O2 Density (m^-3)           79  7  20   0.001 0.0 10** TWOBYTES 80
 7
MSIS_AR         MSIS Ar Density (m^-3)           79  8  20   0.001 0.0 10** TWOBYTES 80
 8
MSIS_N          MSIS N Density (m^-3)            79  9  20   0.001 0.0 10** TWOBYTES 80
 9
MSIS_H          MSIS H Density (m^-3)            79 10  20   0.001 0.0 10** TWOBYTES 8
0 10
MSIS_DENS       MSIS Neutral Density (m^-3)      79 11  20   0.001 0.0 10** TWOBYTES 8
0 11
MSIS_TEMP       MSIS Neutral Temperature (K)     79 12  20   0.1 0.0 TWOBYTES 80 12
MSIS_PRESS      MSIS Neutral Pressure (Torr)     79 13  20  -0.0005 0.0 10** TWOBYTES
80 13
LP_DENS         LP Derived Density (cm^-3)       79 15  20  10.0 0.0 TWOBYTES 80 15
SPHERE_FIX      Sphere Voltage Fixed (V)         78  1   2   0.5  -2000. TWOBYTES 78 2
PLASMAI         Plasma Current (mA)              76  1   2   0.1  -200. TWOBYTES 76 2
```

DEPARTMENT OF DEFENSE

DEFENSE SPECIAL WEAPONS AGENCY
    ATTN: ESA, W SUMMA
    ATTN: EST, K WARE
  2 CY ATTN: TRC

DEFENSE TECHNICAL INFORMATION CTR
  2 CY ATTN: DTIC/OCP

FC DEFENSE SPECIAL WEAPONS AGENCY
    ATTN: FCTT, DR BALADI

DEPARTMENT OF THE ARMY

ELECTRONICS TECH & DEVICES LAB
    ATTN: PULSE POWER CTR
    ATTN: SLCET-D, C THORNTON

DEPARTMENT OF THE NAVY

NAVAL POSTGRADUATE SCHOOL
    ATTN: CODE 61SW, F SCHWIRZKE

NAVAL RESEARCH LABORATORY
    ATTN: CODE 6700, S OSSAKOW
    ATTN: CODE 6750, R MEGER
    ATTN: CODE 6770, G COOPERSTEIN
    ATTN: CODE 6770, R COMMIISSO

NAVAL SURFACE WARFARE CENTER
    ATTN: CODE B-20

DEPARTMENT OF THE AIR FORCE

AIR FORCE OFFICE OF SCIENTIFIC RSCH
    ATTN: DR R BARKER

AIR WEATHER SERVICE, MAC
    ATTN: AWS TECH LIBRARY

DEPARTMENT OF ENERGY

LOS ALAMOS NATIONAL LABORATORY
    ATTN: R REINOVSKY
    ATTN: J BROWNELL

SANDIA NATIONAL LABORATORIES
    ATTN: J HARRIS
    ATTN: J MARTIN
    ATTN: M BUTTRAM
    ATTN: W BEEZHOLD

OTHER GOVERNMENT

CENTRAL INTELLIGENCE AGENCY
    ATTN: OSWR, J PINA

NASA LANGLEY RESEARCH CENTER
    ATTN: J LEE

NATIONAL INSTITUTES OF STANDARDS AND
    TECHNOLOGY
    ATTN: R HEBNER

DEPARTMENT OF DEFENSE CONTRACTORS

APPLIED PHYSICAL ELECTRONICS RESEARCH CTR
    ATTN: DR W NUNNALLY

BERKELEY RSCH ASSOCIATES, INC.
    ATTN: R KARES
    ATTN: S BRECHT

ENERGY COMPRESSION RESEARCH CORP
    ATTN: D S WEIN

FORD MOTOR COMPANY CORPORATION
    ATTN: M MOSBROOKER

FORD MOTOR COMPANY CORPORATION
    ATTN: C NAKAYAMA

GA TECHNOLOGIES, INC.
    ATTN: DOCUMENT CONTROL

JAYCOR
    ATTN: CYRUS P KNOWLES

KAMAN SCIENCES CORP.
    ATTN: D MOFFETT

KAMAN SCIENCES CORPORATION
    ATTN: DASIAC
    ATTN: DASIAC/DARE

LOCKHEED MARTIN VOUGHT SYSTEMS
    ATTN: LIBRARY EM-08

MINNESOTA MINING AND MANUFACTURING CO.
    ATTN: D REDMOND
    ATTN: E HAMPL

MISSION RESEARCH CORP.
    ATTN: B GOPLEN

PRIMEX PHYSICS INTERNATIONAL
  ATTN: C STALLINGS
  ATTN: P SINCERNY

PULSE SCIENCES, INC.
  ATTN: P W SPENCE

TETRA CORP
  ATTN: W MOENY

TEXAS TECH UNIVERSITY
  ATTN: DR M KRISTIANSEN

UNIVERSAL VOLTRONICS CORP
  ATTN: W CREWSON

UTAH STATE UNIVERSITY
  2 CY ATTN: W JOHN RAITT

W J SCHAFER ASSOCIATES, INC.
  ATTN: E ALCARAZ

WESTINGHOUSE STC
  ATTN: DR A H COOKSON

AUBURN UNIVERSITY
  ATTN: M ROSE

UNIVERSITY OF NEW YORK-BUFFALO
  ATTN: R DOLLINGER

UNIVERSITY OF CALIFORNIA-DAVIS
  ATTN: J S DEGROOT